Plasma membrane association and resistosome formation of plant helper immune receptors

Zaiqing Wang [1,#], Xiaoxiao Liu [1,#], Jie Yu [1], Shuining Yin [1], Wenjuan Cai [1], Nak Hyun Kim [2], Farid El Kasmi [3], Jeffery L. Dangl [2] and Li Wan [1,*]

[1] National Key Laboratory of Plant Molecular Genetics, CAS Center for Excellence in Molecular Plant Sciences, Institute of Plant Physiology and Ecology, Chinese Academy of Sciences, Shanghai, China.

[2] Department of Biology and Howard Hughes Medical Institute, University of North Carolina at Chapel Hill, Chapel Hill, NC 27599, USA.

[3] Centre for Plant Molecular Biology (ZMBP), University of Tubingen, 72076 Tubingen, Germany.

[#] Z.W., X.L. contributed equally to this work

*Corresponding author: Li Wan

Email: lwan@cemps.ac.cn

Author Contributions: L.W., J.L.D, Z.W., X.L. designed research. Z.W., X.L., J.Y. S.Y., W.C. performed research. Z.W., X.L., L.W., J.L.D, F.E.K., J.Y., N.H.K. analyzed data. L.W. and J.L.D wrote the paper.

Competing Interest Statement: The authors declare no competing interests.

Classification: Plant biology/immunology/biochemistry

Keywords: Plant immunity/NLR immune receptor/helper NLR/cell death

Abstract

Intracellular plant immune receptors, termed NLRs, respond to pathogen effectors delivered into plant cells. Activation of NLRs typically confers immunity. Sensor NLRs, involved in effector recognition, are either TIR-NLRs (TNLs) or CC-NLRs (CNLs). Helper NLRs, required for sensor NLR signaling, include CC^R-NLRs (RNLs) and a special class of CNLs known as NRCs. Activated TNLs produce small molecules that induce an association between the EDS1/SAG101 heterodimer and the NRG1s helper RNLs. Auto active NRG1s oligomerize and form calcium signaling channels largely localized at the plasma membrane (PM). The molecular mechanisms of helper NLR PM association and effector induced NRG1 oligomerization are not well characterized. We find that both RNLs and NRCs require positively charged residues in the second and fourth helices of their CC^R or CC domain for phospholipid binding and PM association before and after activation, despite conformational changes that accompany activation. We demonstrate that effector activation of TNLs induces NRG1 oligomerization at the PM and that the cytoplasmic pool of EDS1/SAG101 is critical for cell death function. EDS1/SAG101 cannot be detected in the oligomerized NRG1 resistosome, suggesting that additional unknown triggers might be required to induce the dissociation of EDS1/SAG101 from the previously described NRG1/EDS1/SAG101 heterotrimer before subsequent NRG1 oligomerization, or that the conformational changes resulting from NRG1 oligomerization abrogate the interface for EDS1/SAG101 association. Our data provide new observations regarding dynamic PM association during helper NLR activation and underpin an updated model for effector induced NRG1 resistosome formation.

63 **Main Text**

64

65 **Introduction**

66

67 Plants employ both cell surface and intracellular immune receptors to detect pathogens. Cell surface
68 Pattern Recognition Receptors (PRRs) recognize Pathogen-Associated Molecular Patterns (PAMPs) and
69 initiate PAMP-triggered immunity (PTI) (1). Intracellular immune receptors known as Nucleotide-binding
70 Leucine-rich repeat Receptor (NLR) proteins recognize corresponding effectors secreted by pathogens
71 into plant cells and initiate effector-triggered immunity (ETI) (2). Plant NLRs express three main types of
72 N-terminal domains: either a Toll/interleukin-1 receptor (TIR) domain, a coiled-coil (CC) domain, or an
73 RPW8 (Resistance to Powdery Mildew 8)-like CC (CC^R) domain. CC and CC^R domains adopt a conserved
74 structure fold of 4 helical bundle (4HB) with the CC^R expressing an extra N-terminal region (3). TIR-
75 NLR, CC-NLR and CC^R-NLR are known as TNL, CNL and RNL, respectively (4). TNL and CNL
76 recognize pathogen effectors to trigger cell death and immune responses and are thus termed sensor NLRs.
77 Downstream of sensor NLRs, many seed plants also deploy helper NLRs to transduce signals. There are
78 three described classes of helper NLRs. The Activated Disease Resistance 1 (ADR1) family, and the N
79 Required Gene 1 (NRG1) family are highly conserved across the land plant phylogeny (5-7). ADR1s and
80 NRG1s belong to the RNL family and are partially redundant downstream immune mediators of TNLs
81 and some CNLs (8). NRCs are a greatly expanded helper NLR class in several plant families, including
82 the Solanaceae (9). NRCs contain canonical CC domains at their N-termini. In *Nicotiana benthmiana* (*Nb*),
83 three NRCs function redundantly downstream of diverse sensor CNLs to regulate cell death and immune
84 responses (10).

85

86 Upon effector recognition, many tested sensor CNLs and TNLs oligomerize and undergo radical
87 conformational changes. For example, the Arabidopsis CNL AtZAR1 and wheat CNL Sr35 form
88 pentameric resistosomes and function as Ca^{2+} permeable channels to directly induce cell death and defense
89 responses (11-15). In contrast, activated sensor TNLs form tetrameric resistosomes that are holoenzymes
90 cleaving NAD^+ to produce small signaling molecules (16-22). These small molecules bind to the
91 heterodimers of the Enhanced Disease Susceptibility 1 (EDS1) with either Senescence-Associated Gene
92 101 (SAG101), or Phytoalexin Deficient 4 (PAD4) (19, 20). In Arabidopsis, AtEDS1 and AtSAG101
93 form a stable heterodimer and cooperate with the AtNRG1s to mainly control cell death, while AtEDS1

94 and AtPAD4 physically associate and function with the AtADR1s to mainly mediate bacterial growth
95 restriction, resistance and transcriptional reprogramming (6, 7, 19, 20, 23, 24), though there are some
96 overlapping functions (8). The auto-active AtNRG1 mutant and AtADR1 were demonstrated to
97 oligomerize and function as Ca^{2+} permeable channel to induce cell death independent of the lipase-like
98 proteins (3). It is currently unknown whether TNL activation is sufficient to trigger RNL oligomerization
99 and whether EDS1/SAG101 and EDS1/PAD4 are present in NRG1 and ADR1 resistosomes, respectively.

100

101 Sensor NLRs are localized in their resting states to various places in the cell, likely in order to engage
102 with the relevant appropriately localized effectors. Consistent with their proposed Ca^{2+} channel activities,
103 some activated CNLs and RNLs exhibit PM localization (3, 12-15, 25, 26). The Arabidopsis CNL RPM1
104 associates with the PM and remains at the PM after its activation by PM targeted effectors that modify its
105 guardee protein RIN4 (25, 27). The Arabidopsis CNL RPS5 also localizes to the PM via a N-terminal
106 acylation signal and functions at the PM (26). By contrast, AtZAR1 distributes mainly in the cytoplasm
107 in the resting state (13). Upon activation, AtZAR1 moves to, oligomerizes at and presumably protrudes
108 through the PM to form an active Ca^{2+} channel (11, 12, 28). Plant helper NLRs including ADR1s, NRG1s
109 and NRCs contain no predicted acylation signal but still localize at the PM before activation (3, 29, 30).
110 AtNRG1.1 localizes to the PM, partially to ER membranes and in the cytosol when transiently over-
111 expressed in *Nb* (3, 31). Arabidopsis ADR1s mainly localizes at the PM in a phospholipid dependent
112 manner, since depletion of phosphatidylinositol-4-phosphate (PI4P) from the PM by overexpression of
113 the yeast phospholipid-phosphatase Sac1p led to a mis-localization of ADR1 and loss of cell death
114 activities (29). During activation by *Phytophthora infestans* infection, NbNRC4 accumulates at the
115 extrahaustorial membrane (EHM) (30). When activated by sensor NLRs, NbNRC4 forms puncta mainly
116 at the EHM and, to a lesser extent, at the PM; a constitutively autoactive NbNRC4 mutant mainly exhibits
117 PM-associated punctate distribution, similar to autoactivated AtNRG1.1 (3, 30). Given that AtNRG1.1
118 CC^R cell death activity is also affected when co-expressed with the yeast phospholipid-phosphatase Sac1p
119 (29) and that NbNRCs do also not possess any N-terminal acylation site or predicted transmembrane
120 anchor, it is very likely that NRG1s and NRCs also associate with PM in a phospholipid dependent manner.
121 However, how exactly the three subtypes of helper NLRs interact with phospholipids is unknown.

122

123 Here we show that the three classes of helper NLRs directly interact with phospholipids via conserved
124 positively charged residues in the second and fourth helices of their CC^R or CC domain to anchor at the
125 PM in both resting and active states, despite undergoing conformational changes accompanying activation.
126 Consistent with the previously reported activation mimic AtNRG1.1 D485V (hereafter, AtNRG1.1 DV)
127 (3, 31), effector activation of an upstream TNL induces AtNRG1.1 oligomerization and puncta formation
128 at the PM. Interestingly, a cytoplasmic AtEDS1/AtSAG101 fraction is important for the AtNRG1.1 cell
129 death function, but this heterodimer cannot be detected in the oligomerized AtNRG1.1 resistosome. These
130 results suggest that the AtEDS1/AtSAG101/AtNRG1.1 heterotrimer induced by TNL activation
131 represents an intermediate state before dissociation of AtEDS1/AtSAG101 and subsequent
132 oligomerization of AtNRG1.1 or that the conformational changes resulting from AtNRG1 oligomerization
133 abrogate the interface for AtEDS1/AtSAG101 association.

134

135 **Results**

136

137 **Positively charged residues in α4 of the 4HB contribute to NRG1 and NRC phospholipid binding**
138 **and PM localization before and after activation.**

139

140 We previously demonstrated that the AtADR1 CC^R domain binds to phospholipids *in vitro* (29), but it
141 remained unknown which residues in AtADR1 CC^R were responsible for that interaction. Assuming that
142 the ADR1 and NRG1 CC^R domains and potentially the NRC CC could use the same mechanism for
143 phospholipid binding and PM association, we performed sequence alignment with ADR1s, NRG1s and
144 NRCs from Arabidopsis and *Nb* to identify potential conserved, positively charged residues that might
145 bind negatively charged phospholipids. We found an absolutely conserved lysine residue corresponding
146 to K100 in AtNRG1.1 (Figure S1A). This lysine residue is highly conserved in ADR1s, NRG1s and NRCs
147 across different plant species (Figure 1A). We did not observe conservation of this amino acid in AtRPS5
148 which features an N-terminal acylation signal for PM localization, in AtRPM1 which relies largely on
149 association with RIN4 for PM association or in AtZAR1 which mainly localizes in the cytoplasm when
150 overexpressed in *Nb* (Figure S1A and S1B). This observation further suggests a specific and potentially
151 functional role for the AtNRG1.1 K100 equivalent in PM-localization of helper NLRs. Lipid-strip binding
152 assays showed that purified AtNRG1.1 CC^R (aa 1-124) protein specifically binds to phospholipids

153 including PI4P, while K100E completely abolished phospholipid binding. We note that even 2 or 5 times
154 more K100E protein could not restore the binding to AtNRG1.1 CC^R wide-type (WT) level (Figure 1B).
155 K100E was still active in triggering cell death in *Nb*, though this phenotype was weaker than the control,
156 AtNRG1.1 DV (Figure 1C and 1D). Considering that positively charged residues adjacent to K100 may
157 also contribute to phospholipid binding and function, we mutated positively charged residues close to
158 K100 in the α4 helix (Figure S1C). A quadruple mutant K100E/R103E/K106E/K110E (hereafter, g4m)
159 and a penta mutant R99E/K100E/R103E/K106E/K110E (hereafter, g5m) completely suppressed the cell
160 death activity of AtNRG1.1 DV (Figure 1C and 1D). The four single mutants including R99E, R103E,
161 K106E and K110E showed obviously or slightly reduced binding towards phospholipids *in vitro* (Figure
162 1E). Blue-Native PAGE assays showed that K100E and g4m properly oligomerized in the context of
163 AtNRG1.1 DV, while g5m oligomerization was hindered (Figure 1F, also showing equal mutant
164 accumulation on SDS-PAGE immunoblot). Both g4m and g5m strongly affected PM locations of both
165 AtNRG1.1 WT and DV as demonstrated in both Laser Confocal Microscopy (hereafter, confocal) and PM
166 fractionation assays, while K100E had a slight effect (Figure 2A, 2B, 2C and 2D). Given that the cell
167 death function of AtRNG1.1 DV affects protein accumulation, PM fractionation experiments on
168 AtRNG1.1 DV were performed in the context of the previously identified loss-of function mutant ΔN16
169 (deletion of residues 2-16) (Figure 2D) (3). In confocal assays, DV K100E and DV g4m maintained the
170 ability to form puncta at the PM, as observed for AtNRG1.1 DV, but not DV g5m (Figure 2C, S2 and 2E),
171 consistent with their abilities to oligomerize in Blue-Native PAGE assays.

172

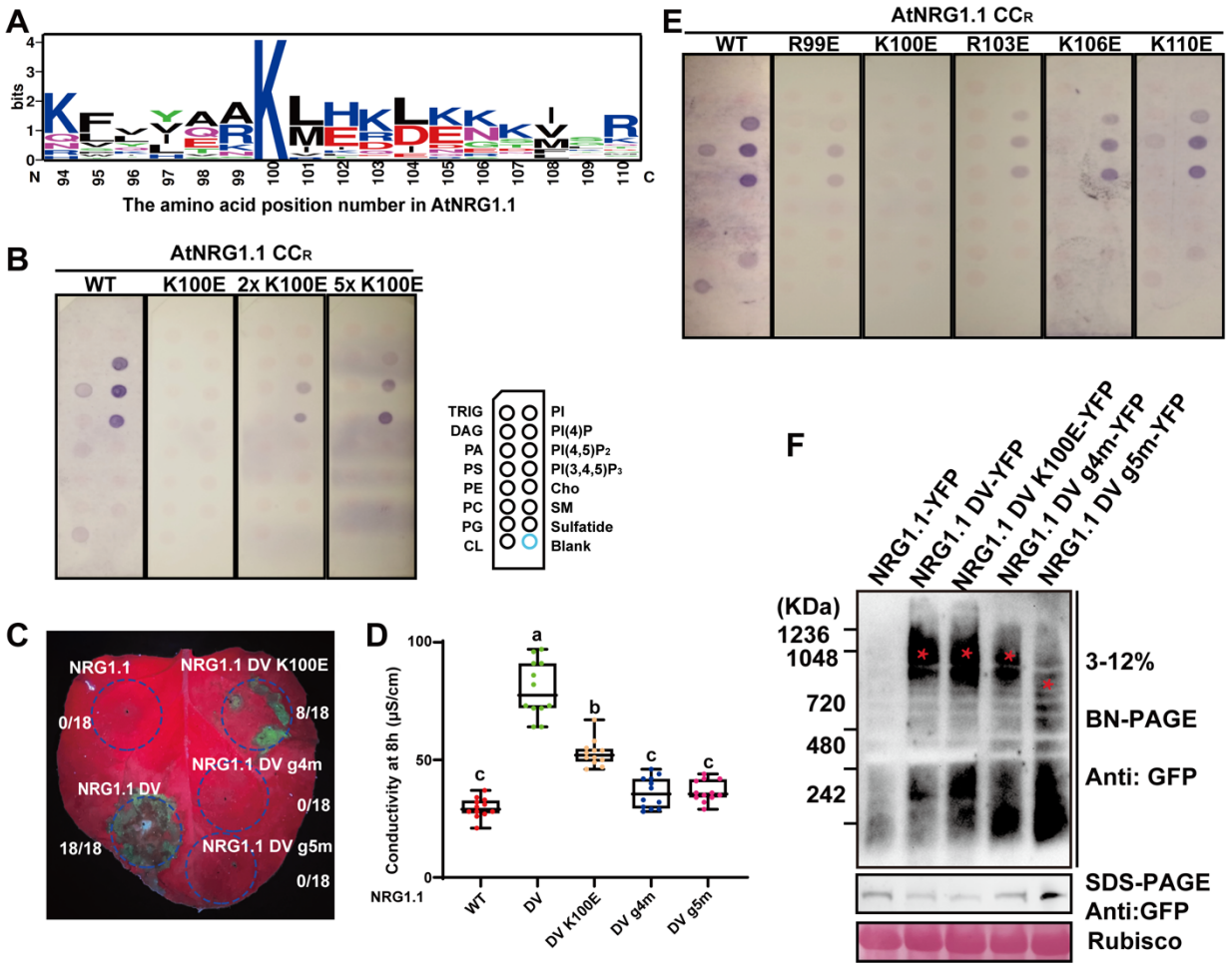

Figure 1 Positively charged residues in the α4 helix of 4HB affect AtNRG1.1 CC^R phospholipid binding and AtNRG1.1 DV function. **(A)** Sequence logos showing the conservation of AtNRG1.1 K100 in three helper NLR families from different plant species. The alignment was performed with ClustalX and sequence logos were generated using WEBLOGO. **(B)** Lipid strip binding assay using purified proteins of AtNRG1.1 CC^R (aa 1-124) and K100E. See *Methods* for lipid definitions. **(C)** Cell death phenotypes of AtNRG1.1 DV and mutants with altered PM localization in *Nb* at 32h post infiltration. (**D**) Quantification of ion leakage from the cell death phenotypes in (C). (**E**) Lipid strip binding assay using purified proteins of AtNRG1.1 CC^R 1-124 and mutants in the α4 helix. **(F)** BN-PAGE analyses of the oligomerization of AtNRG1.1 DV mutants with altered PM localization. Red asterisks indicate oligomerized AtNRG1.1 DV or mutant derivatives.

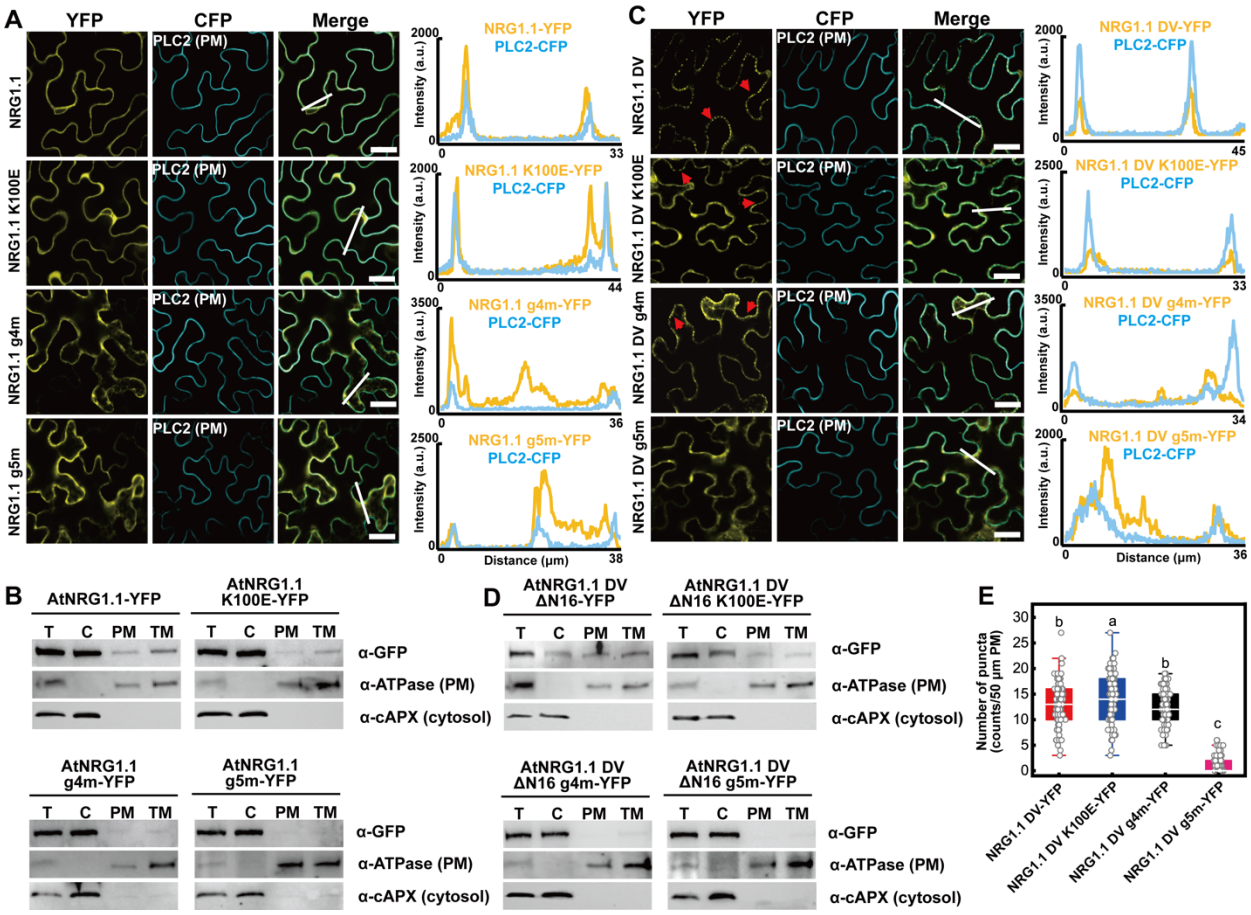

Figure 2 Positively charged residues in the α4 helix of 4HB affect AtNRG1.1 and DV PM association. Confocal microscopy analyses on the mutations of the positively charged residues affecting PM localization of AtNRG1.1 (**A**) and AtNRG1.1 DV (**C**). The indicated proteins fused with a C-terminal YFP were transiently co-expressed with the PM marker PLC2 fused to CFP in *Nb* leaves and confocal images were taken at 32-36h post infiltration. Confocal images are single plane secant views. Merge means merged image between YFP and CFP images. The red arrow heads indicated puncta. Fluorescence intensities were measured along the white line depicted in the merge images. Bars, 25 μm. Membrane fractionation assays on the positively charged residues affecting AtNRG1.1 (**B**) and AtNRG1.1 DV ΔN16 (**D**) protein accumulation at the PM. **(E)**, Quantification of puncta observed in (C).

The corresponding lysine residue is not conserved generally across CNLs, but is conserved in helper NRCs including the NRC negative regulator NbNRCX (Figure S1A) (32). The conserved lysine residue in the α4 helix of the Arabidopsis RNLs corresponds to K84 in NbNRC4. K84E/K87E/K89E/K91E/R94E

(hereafter, c5m) abolished the phospholipid binding of NbNRC4 CC *in vitro* (Figure 3A) and suppressed the cell death activity of NbNRC4 D478V (hereafter, NbNRC4 DV) (Figure 3B, 3C and S3A). Moreover, c5m also attenuated the PM localization of both NbNRC4 WT (Figure 3D and 3E) and NbNRC4 DV (Figure 2F). Given the weak fluorescence signal of NbNRC4 DV due to cell death starting from 24h post infiltration, the confocal assay on NbNRC4DV was performed in the context of the previously identified loss-of-function mutant L9E (Figure 2F) (33). NbNRCX exhibited strong PM localization, while K84E/K89E/K92E/K93E (hereafter, x4m) exhibited reduced PM localization (Figure 2G and 2H). Hence, the positively charged residues in the α4 helix of the 4HB contribute to NRG1 and NRC phospholipid binding and PM localization before and after activation, suggesting a conserved mechanism.

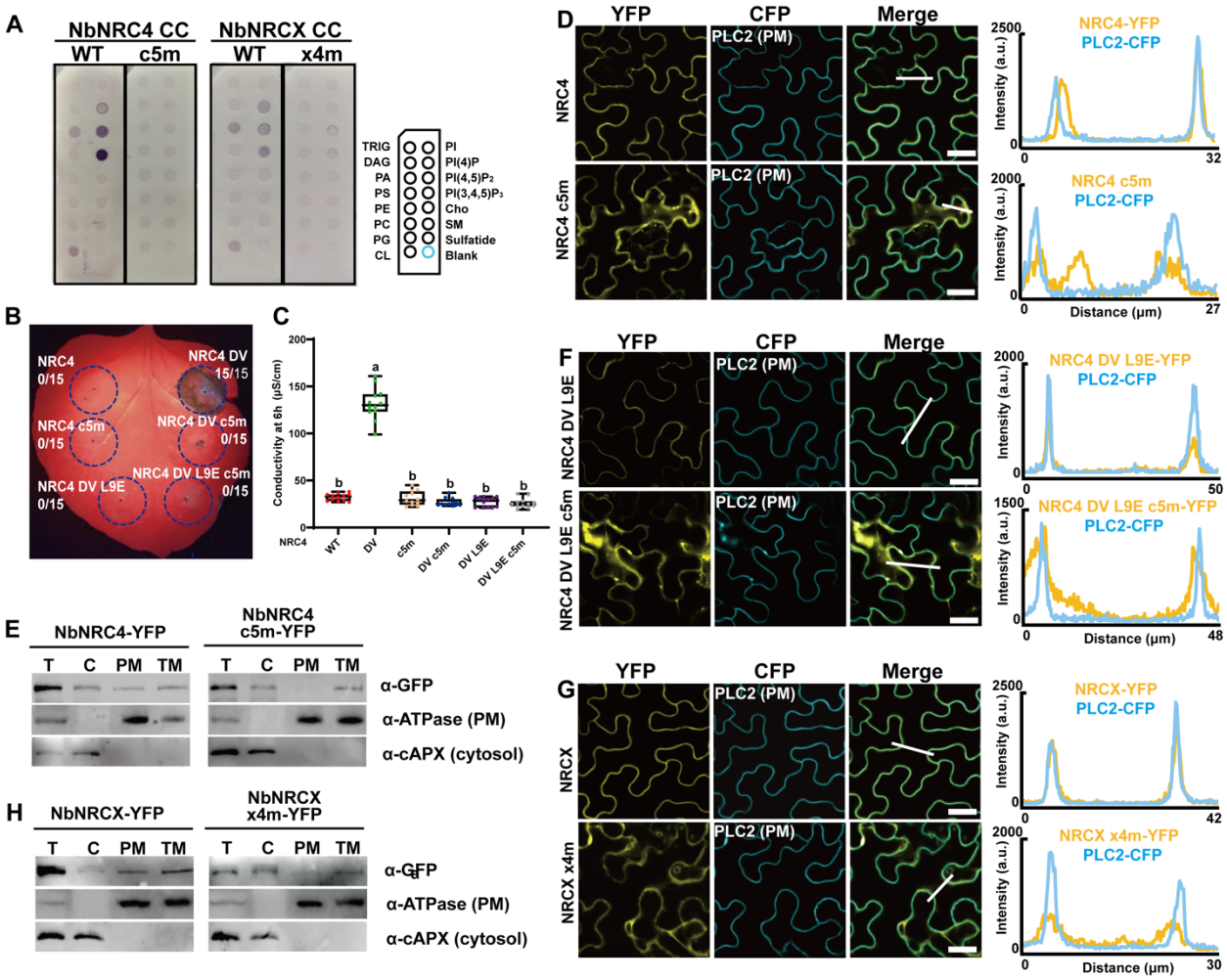

Figure 3 Mutations of the positively charged residues in the α4 helix of 4HB affect NbNRC phospholipid binding, PM localization and function. **(A)** Lipid strip binding assay using purified

215 proteins of NbNRC4 CC (aa 1-127) and its c5m mutant and NbNRCX CC (aa 1-129) and its x4m
216 mutant. See *Methods* for lipid definitions. **(B)** Cell death phenotypes of an NbNRC4 DV activation
217 mimic and mutants with altered PM localization in *Nb* 32h post infiltration. (**C**) Quantification of
218 ion leakage from the cell death phenotypes in (B). Confocal microscopy analyses on the mutations
219 of the positively charged residues affecting PM localizations of NbNRC4 **(D)**, NbNRC4 DV **(F)**,
220 and NbNRCX **(G)**, respectively. The indicated proteins fused with a C-terminal YFP were
221 transiently co-expressed with the PM marker PLC2 fused to CFP in *Nb* leaves and confocal images
222 were taken at 32-36h post infiltration. Images are single plane secant views. Merge means merged
223 images between YFP and CFP images. Fluorescence intensities were measured along the white
224 line depicted in the merge images. Bar, 25 μm. Membrane fractionation assays on the positively
225 charged residues affecting NbNRC4 (**E**) and NbNRCX (**H**) protein accumulation at the PM.

226

227 **Positively charged residues in the α2 and α4 helices of 4HB collectively affect ADR1 PM localization**
228 **before and after activation**

229

230 Mutations in the α4 helix of the 4HB abolished the cell death function of AtNRG1.1 DV and NbNRC4
231 DV, but only partially affected PM localization, indicating that additional residues may also contribute to
232 phospholipid binding. To further investigate if additional residues indeed contribute to phospholipid
233 binding, we chose to focus on AtADR1-L1 because of its distinct PM localization compared to AtNRG1.1
234 and NbNRC4 (29). The conserved lysine residue in the α4 helix corresponds to K99 in AtADR1-L1. The
235 quadruple mutant R98, K99, K102, K105 (hereafter, r4m) in α4 strongly attenuated the phospholipid
236 binding of AtADR1-L1 CC^R *in vitro* (Figure 4A) and AtADR1-L1 D489V (hereafter, AtADR1-L1 DV)
237 cell death activity (Figure 4B and 4C, with protein accumulation controls in S3B). r4m affected the PM
238 localization of both AtADR1-L1 WT (Figure 4D and 4E) and AtADR1-L1 DV (Figure 4F). Further search
239 for conserved positively charged residues in the 4HB of RNLs identified a highly conserved K or R residue
240 corresponding to K30 in AtADR1-L1 and K35 in AtNRG1.1 (Figure S1A and 4G), and the corresponding
241 positions in NRCs are also largely conserved (Figure S1A). A triple mutant of K30 and adjacent positively
242 charged residues, R28E/K30E/K34E (hereafter, r3m), reduced the phospholipid binding of AtADR1-L1
243 CC^R *in vitro* (Figure 4A) and suppressed the cell death phenotype of AtADR1-L1 DV (Figure 4B and 4C),
244 suggesting a critical role of the positively charged residues in the α2 helix. Confocal and membrane

fractionation assays further demonstrated that r3m affected the PM localization of both AtADR1-L1 WT (Figure 4D and 4E) and DV (Figure 4F). The combination of r3m and r4m abolished the phospholipid binding of AtADR1-L1 CC^R *in vitro*, and 2 or 5 times more r3m/r4m protein could not restore the binding to WT level (Figure 4A). Moreover, r3m/r4m abolished the cell death activity of AtADR1-L1 DV (Figure 4B and 4C) and dramatically reduced the PM localization of both AtADR1-L1 WT (Figure 4D and 4E) and DV (Figure 4F, S3C and S3D) to be largely cytoplasmic. Based on an AlphaFold structure model of AtADR1-L1 CC^R in the resting state, the two clusters of positively charged residues involved in r3m and r4m are spatially close to each other (Figure S4A). Hence, the α2 and α4 helices collectively contribute to phospholipid binding and PM localization of ADR1 before and after activation.

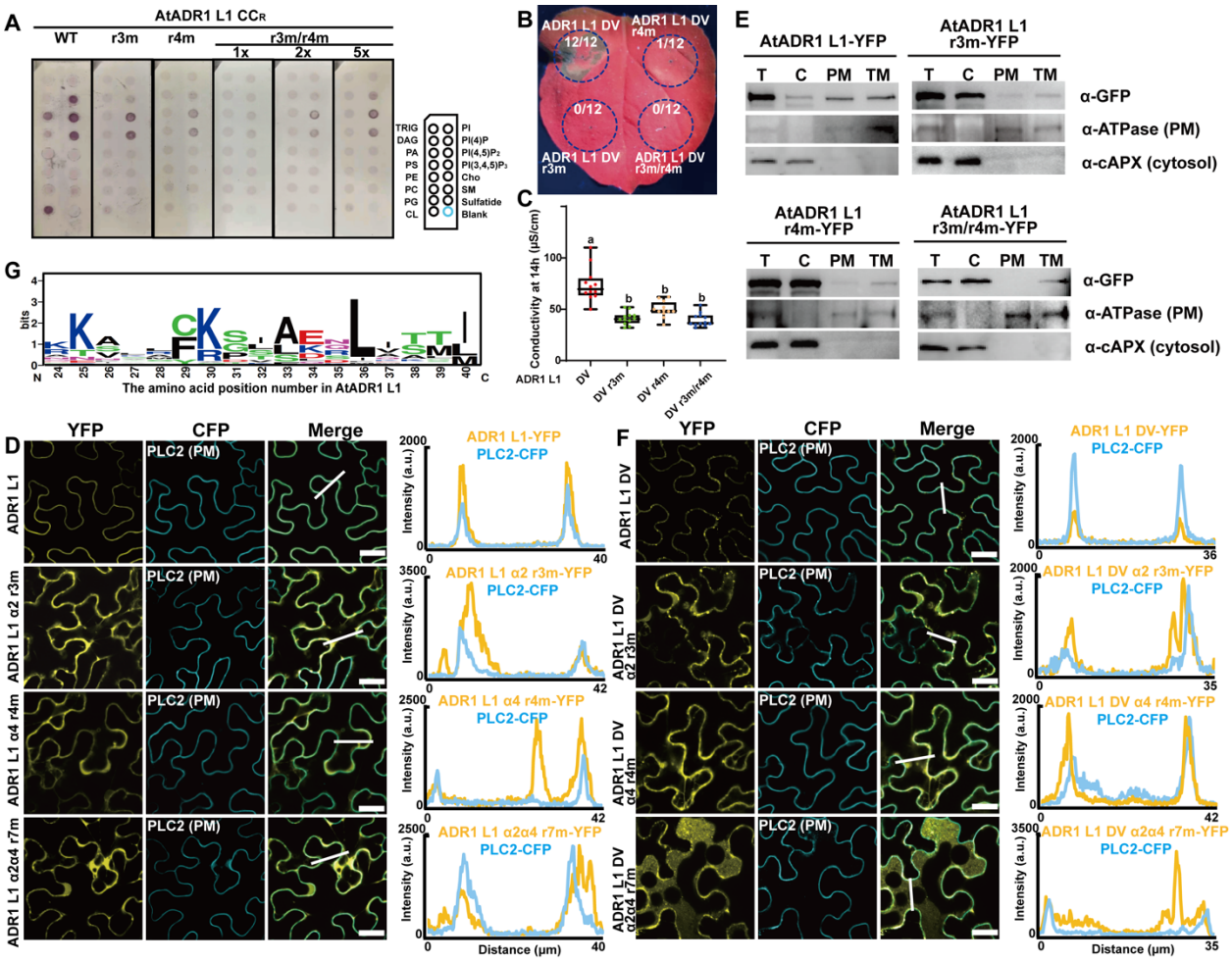

Figure 4 Positively charged residues in the α2 an α4 helices of the 4HB collectively contribute to AtADR1-L1 phospholipid binding, PM localization and function. **(A)** Lipid strip binding assay using purified proteins of AtADR1-L1 CC^R (aa 1-114) and mutant derivatives r3m and r4m. See

259 *Methods* for lipid definitions. **(B)** Cell death phenotypes of AtADR1-L1 DV and mutants with
260 altered PM localization in *Nb* 32h post infiltration. (**C**) Quantification of ion leakage from the cell
261 death phenotypes in (B). Confocal microscopy analyses of the mutations of the positively charged
262 residues affecting PM localizations of AtADR1-L1 **(D)** and AtADR1-L1 DV **(F)**, respectively. The
263 indicated proteins fused with a C-terminal YFP were transiently co-expressed with the PM marker
264 PLC2 fused to CFP in *Nb* leaves and confocal images were taken at 32-36h post infiltration.
265 Confocal images are single plane secant views. Merge means merged image between YFP and
266 CFP images. Fluorescence intensities were measured along the white line depicted in the merge
267 images. Bars, 25 μm. **(E)** Membrane fractionation assays on the positively charged residues
268 affecting AtADR1-L1 protein accumulation at the PM. **(G)** Sequence logos showing the
269 conservation of AtADR1-L1 K30 in RNLs from different plant species. The alignment was
270 performed with ClustalX and sequence logos were generated using WEBLOGO.
271

272 Our data indicate that these helper NLRs are localized to the PM in the resting state via the positively
273 charged residues in the α2 and α4 helices of the 4HB that interact with phospholipids. According to the
274 AtZAR1 activation model, the α1 helix flips out of the 4HB and inserts into the PM upon activation (13)
275 (Figure S4B). The conserved positively charged residue in the α2 helix corresponding to K30 in AtADR1-
276 L1 is located at the very beginning of α2 (Figure S2A) and could still associate with the PM following an
277 AtZAR1-like activation model (Figure S4B). Also, the α4 helix becomes disordered upon oligomerization
278 but maintains contact with the PM (13) (Figure S4B). These conformational changes are likely to allow
279 positively charged amino acids in the α2 and α4 helices to maintain association with the PM post activation.
280 Hence, helper NLRs rely on the conserved positively charged residues in both the α2 and α4 helices of the
281 4HB for phospholipid binding and PM localization before and after activation, despite the conformational
282 changes generated by activation.

283

284 **Effector activation of a TNL induces AtNRG1.1 resistosome formation at the PM**

285

286 Our previous study on auto active AtNRG1.1 DV used different loss-of-function mutations, including
287 L134E that abolished oligomerization, ΔN16 that enhanced oligomerization and D3N/E14Q that
288 specifically blocked Ca^{2+} channel activity (3). It remained unknown whether AtNRG1.1 indeed

289 oligomerizes at the PM following activation by an effector and its corresponding TNL. We transiently
290 expressed AtEDS1/AtSAG101/AtNRG1.1 in *Nb epss* (*eds1a, pad4, sag101a, sag101b*) leaves (6) together
291 with the effector XopQ to reconstitute the TNL Roq1 cell death phenotype (34). AtNRG1.1 WT, but not
292 L134E, ΔN16, D3N/E14Q or g4m, caused cell death (Figure 5A, 5B and S5A). We employed Blue-Native
293 PAGE to investigate AtNRG1.1 oligomerization status following effector activation. AtNRG1.1 WT,
294 ΔN16, D3N/E14Q and g4m oligomerized following Roq1 activation by XopQ, with ΔN16 exhibiting
295 much stronger oligomerization signal than the others; L134E failed to oligomerize (Figure 5C). Hence,
296 g4m specifically affects PM localization of AtNRG1.1, but not oligomerization (Figure 1F, S2 and 2E).
297 These cell death phenotypes and oligomerization states are consistent with the observations using the
298 activation mimic allele AtNRG1.1 DV (Figure 1C, 1D, and 1F) (3). In confocal assays, AtNRG1.1 WT,
299 D3N/E14Q and g4m, which all maintained the ability to oligomerize, also exhibited puncta close to or on
300 the PM, and ΔN16 displayed enhanced puncta; the loss-of-oligomerization mutant L134E exhibited no
301 obvious puncta formation compared to AtNRG1.1 WT (Figure 5D-5I and S5B). These data demonstrate
302 that effector activation of a TNL induces AtNRG1.1 resistosome formation at the PM and that AtNRG1.1
303 DV faithfully mimics the functionality of effector activated AtNRG1.1.

304

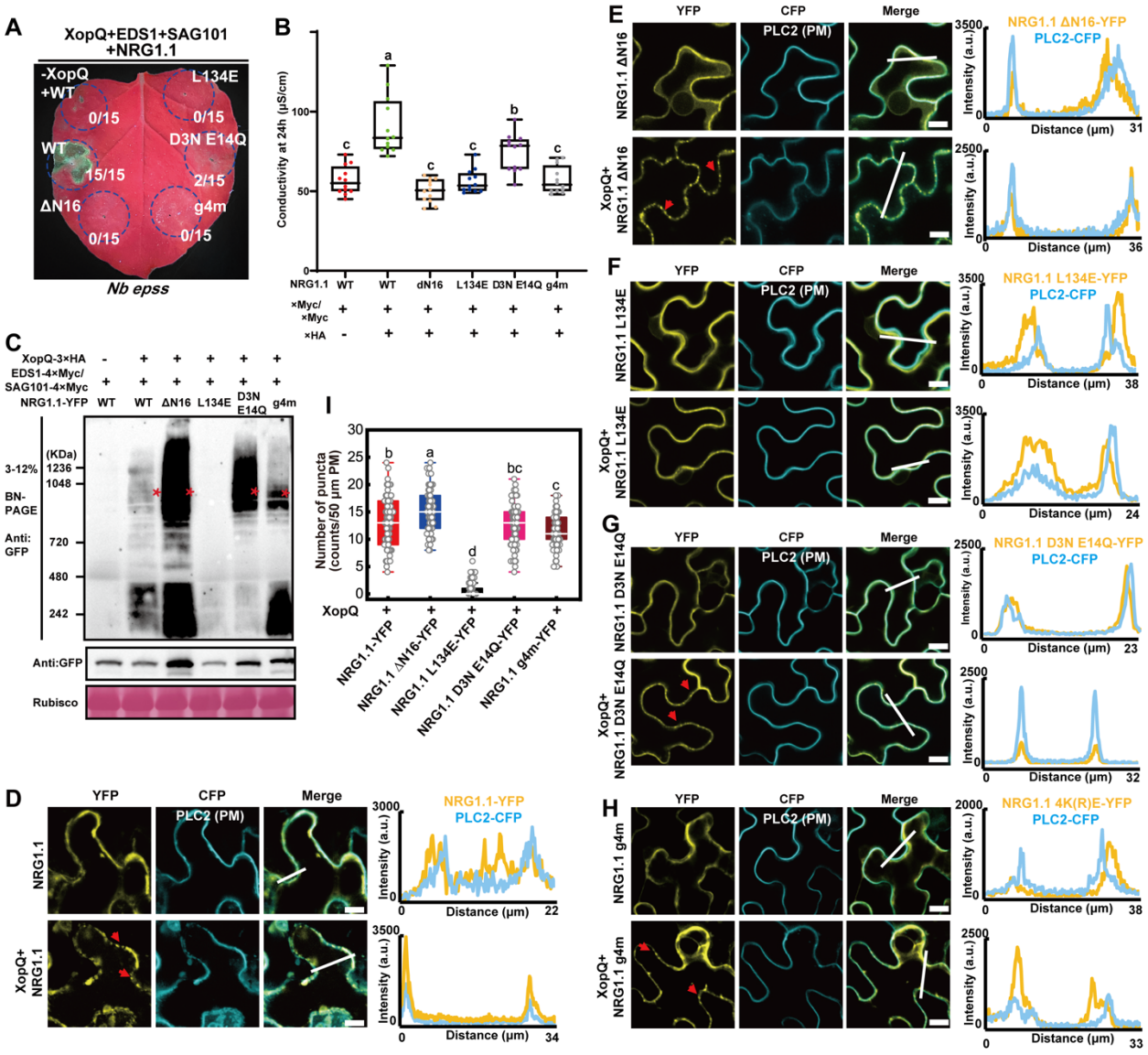

Fig. 5 Effector induced AtNRG1.1 oligomerization and enhanced puncta formation at the PM. **(A)** XopQ-triggered cell death phenotypes in *Nb epss* when co-expressed with AtEDS1, AtSAG101 and AtNRG1.1 mutants 48h post infiltration. (**B**) Quantification of ion leakage from the cell death phenotypes in (A). **(C)** BN-PAGE showing the oligomerization status of AtNRG1.1 mutants in (A). Red asterisks indicate oligomerized AtNRG1.1. Confocal microscopy assays showing PM localization and puncta of AtNRG1.1 **(D)**, derivative alleles ΔN16 **(E)**, L134E **(F)**, D3N/E14Q **(G)** and g4m **(H)** before and post-activation via XopQ expression when co-expressed with AtEDS1 and AtSAG101. The indicated proteins fused with a C-terminal YFP were transiently co-expressed with the PM marker PLC2 fused to CFP in *Nb* leaves and confocal images were taken at 32-36h post infiltration. Confocal images are single plane secant views. Images are single plane secant

316 views. Merge means merged images between YFP and CFP images. The red arrow heads indicated
317 puncta. Fluorescence intensities were measured along the white line depicted in the merge images.
318 Bar, 10 µm. (**I**) Quantification of puncta as observed in (D-H).

319

320 **The cytoplasmic pools of AtEDS1 and AtSAG101 mediate cell death but are not detectable in the**
321 **oligomerized AtNRG1.1 resistosome**

322

323 AtEDS1 and AtSAG101 are localized to the nucleus and the cytoplasm (35, 36). We investigated whether
324 enforced nuclear and cytoplasmic distribution of AtEDS1 and AtSAG101 could affect the cell death
325 phenotype using co-expression complementation assays in *Nb epss* plants. Expression of AtEDS1 and
326 AtSAG101 with a nuclear export signal (NES) slightly attenuated XopQ-TNL Roq1 dependent cell death
327 comparable to wild type AtEDS1 and AtSAG101 (Figure 6A, 6B, and S6), which agrees to some extent
328 with previous finding showing that co-expression of NES-tagged Solanaceae EDS1 with Solanaceae
329 SAG101 blocks XopQ trigged cell death function in *Nb epss* (37). By contrast, AtEDS1 and AtSAG101
330 with a nuclear localization signal (NLS) did not support cell death in this assay (Figure 6A, 6B, and S6).
331 These data suggest that the cytoplasmic pools of AtEDS1 and AtSAG101 activate AtNRG1.1 and are
332 critical determinants of XopQ-activated cell death responses, which is consistent with a recent study
333 showing that different TIR domains preferentially signal cell death via the cytosolic pool of EDS1 in
334 Arabidopsis (38). Given that TIR-dependent signals induce the formation of
335 AtEDS1/AtSAG101/AtNRG1 heterotrimers (20), we performed BN-PAGE to further investigate if
336 AtEDS1 and AtSAG101 are subsequently retained in the oligomerized AtNRG1.1 resistosome.
337 AtNRG1.1 ΔN16 oligomerized in a XopQ-dependent manner following activation of the Roq1 TNL when
338 co-expressed with AtEDS1 and AtSAG101, while AtNRG1.1 ΔN16/L134E was not responsive to XopQ
339 (Figure 6C and S7). However, in samples expressing AtNRG1.1 ΔN16, with or without XopQ, or
340 AtNRG1.1 ΔN16/L134E plus XopQ, we did not detect oligomerization of AtEDS1 (Figure 6C, StrepII
341 immunoblot) or AtSAG101 (Figure 6C, Flag immunoblot) at the high molecular weight regions
342 corresponding to AtNRG1.1 oligomers. We ruled out the tag effect for the negative results by detecting
343 oligomerization of AtRNG1.1 ΔN16 with the same epitope tag as either AtEDS1 or AtSAG101 in a single
344 gel at three different time points 26h, 32h, and 42h post infiltration (Figure 6C and S7). Hence AtEDS1
345 and AtSAG101 could not be detected in the oligomerized AtNRG1.1 resistosome in this cell death

346 reconstitution assay in *Nb epss*. One hypothesis is that additional signals may be required to trigger the
347 dissociation of AtEDS1/AtSAG101 and subsequent oligomerization of AtNRG1.1 after TIR-induced
348 AtEDS1/AtSAG101/AtNRG1.1 heterotrimer formation (Figure 6D).

349

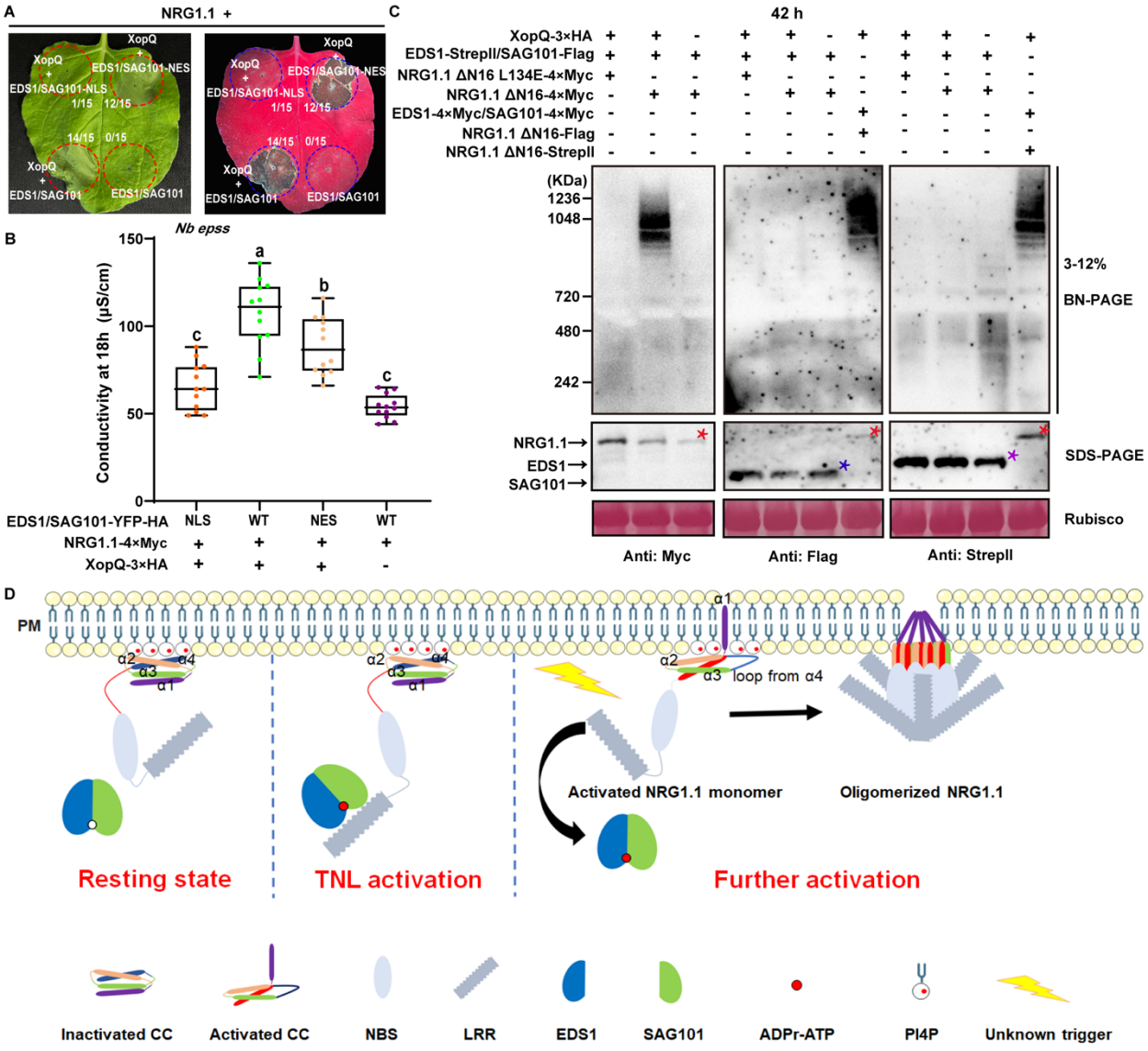

350

351 **Fig. 6** AtEDS1 and AtSAG101 cannot be detected in the oligomerized AtNRG1.1 resistosome. **(A)**
352 The cytoplasmic pool of EDS1/SAG101 activates NRG1.1 to induce cell death. EDS1/SAG101-
353 NLS, EDS1/SAG101-NES, or EDS1/SAG101 with a C-terminal YFP-HA tag were transiently co-
354 expressed with NRG1.1-4×Myc and XopQ-4×Myc in *Nb epss*. Cell death phenotypes were
355 photographed 42h post infiltration. (**B**) Quantification of ion leakage from the cell death
356 phenotypes in (A). **(C)** EDS1/SAG101 do not co-migrate with NRG1.1 upon XopQ activation in

357 BN-PAGE assays. *Agrobacteria* mixes carrying the indicated expression constructs were co-
358 infiltrated into *Nb epss*. Total protein extracts were resolved by BN-PAGE and SDS-PAGE 42h
359 post infiltration. Target bands were immunoblotted with appropriate antibodies. Red asterisk
360 indicates the protein band of NRG1.1. Purple and blue asterisks indicate EDS1 and SAG101 bands,
361 respectively. **(D)** An updated model on PM association and effector-induced oligomerization of
362 NRG1.
363
364 **Discussion**
365
366 PM localization was required for Ca^{2+} channel formation or immune function of RNLs and many CNLs
367 (3, 12, 14, 15, 25, 26, 29, 30). Helper NLRs, including NRG1s and ADR1s, exhibited significant PM
368 location before activation (or the extra-haustorial membrane in the case of NbNRC4) and are further
369 enriched and concentrated at the PM after activation (3, 29-31). Mechanisms driving helper NLR PM
370 localization remained largely unclear.
371
372 In plants, PI4P is the main driver of PM electrostatics (39, 40). Phosphatidic acid (PA) and
373 phosphatidylserine and PI(4,5)P_2 also contribute to PM (inner leaflet) surface charges, but to a lesser
374 extent. We generated mutations in the conserved positively charged residues in the α2 and α4 helices of
375 helper NLR 4HBs. These mutations attenuated phospholipid binding *in vitro* and PM association *in vivo*;
376 they also abolished cell death function. Another 4HB-containing membrane pore forming protein, the
377 animal mixed lineage kinase domain-like (MLKL), specifically interacts with phospholipids for PM
378 localization and function (41). A recent study showed that *Mycobacterium tuberculosis* inhibits pyroptosis
379 by secreting a phospholipid phosphatase that localizes at the host PM to dephosphorylate PI4P and
380 PI(4,5)P_2 and suppresses the PM association and pore function of activated Gasdermin D (42). Hence
381 phospholipid-binding mediated PM association is a conserved mechanism for membrane pore forming
382 proteins. It remains to be investigated whether plant pathogens employ similar phospholipid phosphatases
383 to perturb the PM localization and thus the function of helper NLRs.
384
385 We provide mechanistic insights into the dynamics of PM association during plant helper NLR activation.
386 In the absence of pathogen infection, interactions of the α2 and α4 helices of the N-terminal 4HB anchor

387 a significant fraction of plant helper NLRs at the PM. Upon activation by senor NLRs, helper NLRs
388 undergo dramatical conformational changes and further concentration at the PM; they still rely on the α2
389 and α4 helices to associate with the PM for function (Figure 5C).

390

391 The RNL helper ADR1s and NRG1s contain an RPW8-like CC^R domain at their N-termini. In addition to
392 the 4HB, the CC^R domain has an extra N-terminal region that was previously predicted to be responsible
393 for CC^R membrane targeting (43). Deletion of the extra N-terminal region did not affect PM localization
394 of the activation mimic allele AtNRG1.1 DV (3) or effector-activated AtNRG1.1 (Figure 4D). Mutation
395 of the positively charged residues in the α4 helix affected PM localization of AtNRG1.1 WT and the DV
396 allele (Figure 1D and 1E). Despite the absolute conservation of AtNRG1.1 K100 in the CC^R domain of
397 ADR1s and NRG1s, it is not conserved in RPW8 (Figure S1A), indicating a different PM association
398 mechanism for RPW8.

399

400 AtNRG1.1 K100 is highly conserved in RNL and NRC helpers, but is less well conserved in sensor CNLs
401 (Figure S1A). In contrast to RNL helpers, the well-studied sensor CNL AtZAR1 that also functions as a
402 PM-localized Ca^{2+} channel post activation, localizes mainly in the cytoplasm before activation (Figure
403 S1B) (12, 13). In contrast, the sensor CNL AtRPM1 interacts with the PM-localized guardee RIN4,
404 localizes to and signals from the PM (25, 44, 45); the senor CNL AtRPS5 localizes to the PM via N-
405 terminal acylation signal and functions at the PM (26). Thus, sensor NLRs express variable resting state
406 subcellular distributions, likely reflecting the subcellular localization of the pathogen effectors they detect.
407 Hence, helper NLR use a specific mechanism for enrichment at the PM before activation, which may be
408 critical for rapid calcium signal induction upon activation of ETI. It remains to be determined whether
409 other CNLs also use similar phospholipid binding mechanisms to determine or enhance PM localization.

410

411 PTI and ETI function cooperatively and potentiate each other (46, 47), but the mechanisms that
412 interconnect PTI and ETI remain unclear. The EDS1/PAD4/ADR1 module associates with some PM
413 located PRRs and is required for PTI (48-50). NbNRC3 mediates the hypersensitive cell death caused by
414 the cell-surface receptor Cf-4 recognizing the apoplastic fungal effector Avr4 (51). An enriched or
415 constitutive PM-bound pool of helper NLRs are potentially important for their efficient activation by PTI
416 signals and the cooperative function between PTI and ETI. We demonstrated that NbNRCX, a negative

417 regulator of NbNRC2 and NbNRC3 (32), also uses the conserved positively charged residues in the α4
418 helix of 4HB for PM association (Figure 2D). We propose that the PM location of NbNRCX is important
419 for its negative regulation of activated NbNRC2 and NbNRC3 at the PM, perhaps via the formation of
420 mixed and thus 'poisoned' oligomers.

421

422 Effector activation of sensor CNL triggers helper NRC oligomerization, and sensor CNLs are not present
423 in the NRC oligomer complex (52, 53). We present data that ETI activated via the effector XopQ and the
424 TNL Roq1 induces RNL AtNRG1.1 oligomerization and puncta formation at the PM (Figure 4). A recent
425 study showed that in Arabidopsis the oligomerization of AtNRG1.2 requires not only effector-mediated
426 activation of a TNL, but also activation of PTI (54). Our data show that the cytoplasmic pool of
427 AtEDS1/AtSAG101 mediates the cell death response, but that neither are readily detectable in the effector-
428 induced oligomerized AtNRG1.1 resistosome (Figure 5A and 5B). This is in contrast to the recent
429 observation of NRG1.2/EDS1/SAG101 hetero-oligomers that were detectable only after
430 immunoprecipitation of NRG1.2 (54). The combined data suggest that additional unknown triggers may
431 be required to induce AtEDS1/AtSAG101 dissociation from the AtNRG1.1/AtEDS1/AtSAG101
432 heterotrimer and subsequent AtNRG1.1 oligomerization at the PM (Figure 6D), or that the conformational
433 changes resulting from oligomerization abrogate the interface(s) required for AtEDS1/AtSAG101 co-
434 association. It is also possible that NRG1/EDS1/SAG101 hetero-oligomers are transient, while we
435 detected a latter stage of the oligomerized NRG1 resistosome after EDS1/SAG101 disassociate. The
436 putative role of PTI in facilitating either the rare NRG1.2/EDS1/SAG101 hetero-oligomers or oligomeric
437 NRG1 resistosome formation at the PM requires future investigation.

438

439 **Materials and methods**

440

441 **Plant growth conditions**

442 *Nb* WT and *Nb epss* plants were grown in a growth chamber at 25°C under a 16 h/8 h light/dark
443 cycle with relative humidity at 55±10%.

444

445 **Vector construction**

446 The coding sequences (CDS) of *AtNRG1.1* (At5g66900), *AtEDS1* (At3g48090), *AtSAG101*
447 (At5g14930), *AtADR1-L1* (At4g33300) and *PLC2* (At3g08510) were amplified using specific
448 primers from the Arabidopsis ecotype Col-0, and the CDS of *NbNRC4* (NbS00016103g0004,
449 2,464 bp) and *NbNRCX* (NbS00030243g0001, 2,619 bp) were amplified by PCR from *Nb*. The
450 resulting PCR fragments were cloned into a modified pUC19 vector with the gateway compatible
451 recombination sites (attL1/attL2). The StrepII tag sequence was fused to the 3' cDNA of *AtEDS1*
452 to obtain an *AtEDS1-StrepII* entry clone. *AtNRG1.1 Δ16* was PCR-amplified using the CDS of
453 *AtNRG1.1* as a template and then cloned into the entry vector pUC19. Other *AtNRG1.1* variants
454 were generated using Fast Mutagenesis System protocol (Transgene). *XopQ* with *attL1/attL2*
455 sequences was synthesized into a pUC18 plasmid (Genescript). *XopQ* was introduced to
456 expression vectors pGWB614 and pGWB617 to obtain *35S:: XopQ-3×HA* and *35S:: XopQ-*
457 *4×Myc* constructs, respectively. *AtEDS1* and *AtEDS1-StrepII* were recombined into pGWB617
458 (35S promoter, C-terminal 3×Myc) and pGWB2 (35S promoter, no tag), respectively. *AtSAG101*
459 was introduced to pGWB11 (35S promoter, C-terminal Flag) and pGWB617. *AtNRG1.1* and the
460 mutants were introduced into pGWB641 (35S promoter, C-terminal EYFP), pGWB617, the
461 modified vectors pEarleyGate-Flag (35S promoter, C-terminal Flag) and pEarleyGate-StrepII (35S
462 promoter, C-terminal StrepII) to express fusion proteins with desired tags. All target sequences
463 were introduced into expression vectors using LR reactions (Life Technologies). *35S::AtEDS1-*
464 *YFP-HA-NLS* (or *NES*) and *35S::AtSAG101-YFP-HA-NLS* (or *NES*) expression constructs were
465 obtained using LR to recombine pUC19-*AtEDS1*, pUC19-*AtSAG101* with modified vectors
466 pEarleyGate 101-NLS and pEarleyGate 101-NES (55). *NbNRC4* and *NbNRCX*, and their mutants
467 were introduced into the 35S-omega-driven destination vector pEarlyGate with a C-terminal YFP-
468 HA. The CDS of plasma membrane marker PLC2 (At3g08510) and endoplasmic reticulum marker
469 VMA12 (At5g52980) were amplified from Col-0 and subsequently cloned into PUC19/Kan vector

470 including attR1/attR2 sites. *PLC2-CFP* expression vector and *VMA12-RFP* were generated by
471 Golden Gate assembly with 35S-driven pEarly101 with a C-terminal CFP and 35S-driven
472 pGWB257 with a C-terminal RFP, respectively. The obtained expression constructs were
473 transformed into *Agrobacterium tumefaciens* GV3101 via electroporation for transient expression
474 in *Nb*.
475
476 **Transient expression in *Nb***
477 *Agrobacteria* (GV3101) carrying the constructs were grown overnight in LB with suitable
478 antibiotics. 3 mL of *Agrobacterium* culture was centrifuged and resuspended in MES buffer (10
479 mM $MgCl_2$, 10 mM MES pH 5.6, 150 μM acetosyringone). *Agrobacteria* were incubated at room
480 temperature for 1h and infiltrated into the leaves of 5-week-old *Nb or Nb epss* at specific OD_{600}
481 values. *Agrobacteria* containing the *P19* construct was co-infiltrated at OD of 0.1. Cell death
482 phenotypes were photographed at indicated time point.
483
484 **Ion leakage assays**
485 Four leaf discs 8mm in diameter were harvested 24h after transient expression in *Nb* leaves. Leaf
486 discs were washed for 1h in 10 mL ultrapure water, transferred into 15-mL tubes containing 6 mL
487 ultrapure water. Conductivity was measured using a conductivity meter (FiveGo Cond meter F3,
488 METTLER TOLEDO) at indicated time point. 3 biological repeats and 4 technical repeats were
489 performed. Statistical analysis was performed via Tukey's HSD (honestly significant difference)
490 using GraphPad Prism 8. Different letters indicate statistically significant differences.
491
492 **Total protein extraction and western blot analysis**
493 Three 8 mm leaf discs were harvested and ground to powder in liquid nitrogen. Total protein was
494 extracted with 100 μL extraction buffer (20 mM Tris–HCl pH 8.0, 5 mM EDTA, 1% SDS, 10 mM
495 DTT). Lysate was boiled at 95 °C with 1×protein loading buffer for 10 min. The total protein
496 extract was cleared by centrifuge at 13,000 *g* for 10 min. Then the supernatant was separated by
497 10% SDS–PAGE gels and detected with corresponding antibodies. Antibodies used for
498 immunoblotting include anti-GFP (#G1544, Sigma), anti-HA (#11867423001, Roche), anti-Myc
499 (#M4439, Sigma), anti-Flag (#SAB4301135, Sigma), anti-StrepII (#ab76949, Abcam), and HRP-

500 conjugated antibodies (#IMR-GtxMu-003-DHRPX, #IMR-GtxRb-003-DHRPX, #GtxRt-003-
501 DHRPX, Jackson).
502
503 **BN-PAGE**
504 BN-PAGE was performed as previously described with slight modifications (3). 3 leaf disks (5
505 mm diameter) were homogenized with liquid nitrogen. 1× NativePAGE™ Sample Buffer
506 (BN2008, Invitrogen™) with 1× protease inhibitor cocktail was added to the homogenized
507 samples. The mixed samples were centrifuged at 20,000 *g* for 30 min at 4°C. Native PAGE™ 5%
508 G-250 Sample Additive (BN2004, Invitrogen™) was added to the supernatant at a final
509 concentration of 0.125%. Proteins were separated by Native PAGE™ Novex® 3–12% Bis-Tris
510 Gels (BN1001, Invitrogen™) and transferred to PVDF membrane using an eBlot™ L1 transfer
511 system (GenScript). The target proteins were probed with corresponding antibodies.
512
513 **Confocal microscopy analyses**
514 For *Agrobacterium*-mediated transient expression in *Nb*, OD_{600} cultures were adjusted to 0.1 of
515 P19, 0.2 of PLC2, and 0.2 of AtNRG1.1, AtADR1-L1, NbNRC4 or NbNRCX. *Agrobacteria*
516 mixtures were infiltrated into young leaves of 4-6 weeks old *Nb* plants. For transient expression in
517 *Nb epss*, the OD_{600} was adjusted to 0.1 of P19, 0.1 of AtEDS1 and AtSAG101, and 0.2 of
518 AtNRG1.1 and PLC2 (VMA12-RFP or RFP), and 0.001 for XopQ. Agrobacteria mixtures were
519 infiltrated into young leaves of 4-6 weeks old *Nb epss* plants. Leaves were imaged for protein
520 localization analyses between 36h-48h post infiltration. Confocal images were taken on a confocal
521 laser scanning microscope LSM880 from Zeiss (Oberkochen, Germany) using the ZENblack
522 software, via a Zeiss-C-Apochromat 20×/0.8 A20650-9901 objective or a Zeiss-W-Plan-
523 Apochromat 421462-9900 objective. YFP was excited using a 514 nm laser and the emission
524 spectrum was between 516-556 nm; CFP was excited with a 458 nm laser and the emission
525 spectrum was between 463-513 nm. Focal plane images were processed with the ZEN blue
526 software (Zeiss) for adjustment of brightness and contrast.
527
528 **Membrane fractionation assays**
529 Plasma membrane protein isolation was carried out by slightly modifying a previously described
530 protocol (3).In brief, sucrose buffer [20mM Tris (pH 8.0), 0.33M sucrose, 1mM EDTA, 5mM DTT

531 and 1x Sigma plant protease inhibitor cocktail] was added to the homogenized tissue at a ratio of
532 5 uL per mg (FW) tissue. The extract was centrifuged at 2,000 x *g* for 5 minutes at 4°C, then the
533 supernatant was transferred to a new tube and designated as total protein (T). Cytoplasmic fraction
534 (C) was prepared by harvesting the supernatant after spinning the total protein fraction at 20,000
535 x *g* for 1h at 4°C. The total membrane fraction (TM) was prepared from the resulting pellet by
536 resuspending in 200 uL of buffer B (Minute™ plasma membrane protein isolation kit, Invent
537 Biotechnologies). Centrifuged at 7,800 x *g* for 15 min at 4°C, then the supernatant was transferred
538 to 2 mL Eppendorf tube and mixed with 1.6 mL cold PBS buffer mixed by vortexing and spun at
539 16,000 x *g* for 1h at 4°C to pellet the plasma membrane fraction. The pellet was resuspended with
540 sucrose buffer in 4 times less volume than the soluble fraction. The resulting fraction was labelled
541 as the plasma membrane-enriched/microsomal fraction (PM). Proteins fractions were run on SDS-
542 PAGE gels and analyzed by western blotting.
543
544
545 **Sequence alignment of helper NLR homologs**
546 AtNRG1.1 and AtNRG1.2 (At5g66910.1) were used to identify NRG1 homologs in the predicted
547 protein databases including Solanaceae Genomics Network (SGN) and Integrated Microbial
548 Genomes (IMG). Similarly, AtADR1 (At1g33560.1), AtADRL1-L1 and AtADRL1-L2
549 (At5g04720.1 were used to identify ADR1 homologs. NbNRC2 (NbS00018282g0019.1 and
550 NbS00026706g0016.1), NbNRC3 (NbS00011087g0003.1), NbNRC4 (NbS00002971g0007.1 and
551 NbS00016103g0004.1) and NbNRCX (NbS00030243g0001.1) were used to identify NRC-helper
552 clade homologs in the SGN database. Top hits from BLASTP search results in different plant
553 species were collected for further analyses. Homologs with protein sequence identity of more than
554 50% were aligned in their CC or CC^R domains by CLustalW. The gene ID of homologs used in
555 the alignment were listed in Table S1.
556
557 **Sequence logos visualization**
558 Sequence logos of the identified conserved amino acid site in CC or CC^R domain of helper NLRs
559 were generated by the online software WEBLOGO (http://weblogo.berkeley.edu/logo.cgi) (56).
560
561 **Protein expression and Lipid-strip binding assays**

562 Sequences of AtNRG1.1 CC 1-124 (WT, R99E, K100E, R103E, K106E and K110E) were
563 subcloned into the pET24a plasmid with a N-terminal 6×His and a C-terminal StrepII tag. Proteins
564 were expressed in *E. coli* BL21 (DE3) cells using the autoinduction method (57). Cell pellets were
565 resuspended and lysed in buffer containing 50 mM HEPES (pH 8.0), 300 mM NaCl, 2 mM DTT
566 and 1 mM PMSF. After sonication and centrifugation at 20,000 *g* for 60 minutes, supernatant was
567 loaded onto a nickel HisTrap 5 mL column (GE Healthcare) pre-equilibrated with 20 mL of the
568 wash buffer (50 mM HEPES pH 8.0, 300 mM NaCl, 30 mM imidazole) at a 3 mL/min rate. The
569 bound proteins were eluted with elution buffer (50 mM HEPES pH 7.5, 300 mM NaCl, 500 mM
570 imidazole), and further purified using size exclusion chromatography (Superdex 200 HiLoad
571 16/600 column) pre-equilibrated with the buffer containing 10 mM HEPES pH 7.5, 150 mM NaCl
572 and 1mM DTT. The peak fractions were confirmed by SDS-PAGE and pooled for Lipid-strip
573 binding assays.
574
575 Proteins of AtADR1 L1 CC^R 1-114 (WT, r3m, r4m and r3m/r4m), NbNRC4 CC 1-127 (WT and
576 c5m) and NbNRCX CC 1-129 (WT and x4m) were expressed and purified in the human embryonic
577 kidney cell line 293F. The corresponding cDNAs of these constructs were subcloned into the
578 pMlink vector with a N- terminal proteinA and SUMOstar tag and a C-terminal Flag tag. Plasmids
579 were transfected into 293F cells using the polyethyleneimine (PEI) method (58). Cells were grown
580 in Union-293 Chemically Defined Medium (Union Bio) and were routinely maintained at
581 exponential phase in 1000-mL shaker flasks. The flasks were agitated at 130 rpm at 37°C in a
582 humidified condition containing 5% CO2. Cells were pelleted at 8000 x g at 4°C for 5 minutes
583 using centrifugation at 72h after transfection. Pellets were resuspended and lysed in lysis buffer
584 (50 mM Tris-Hcl, 300 mM NaCl, 0.5 mM EDTA, 10 % (v/v) Glycerol, 2 mM DTT, 1 mM PMSF,
585 5 mM ATP, 2 mM MgSO4, 1 % (v/v) Cocktail, 0.9 % (m/v) DNase I and 0.2 % (m/v) CHAPS,
586 pH 7.5). After vibration at 4°C for 60 minutes and centrifugation at 20,000 x g for 60 minutes,
587 supernatant was loaded onto 6 mL immunoaffinity chromatography column with 1 mL IgG beads
588 (Smart-Lifesciences) pre-equilibrated with 50 mL of the wash buffer (50 mM Tris-Hcl, 300 mM
589 NaCl, 0.5 mM EDTA, 10 % (v/v) Glycerol, pH 7.5). The bound proteins were digested by ULPI
590 enzyme, and further the flow-through containing approved proteins were collected and
591 concentrated for Lipid-strip binding assays.
592

593 Lipid-strip binding assays were performed according to the manufacturer's instructions (Echelon
594 Biosciences, Salt Lake City, UT, USA). Briefly, the PIP-strip membranes were blocked overnight
595 at 4 °C in blocking buffer containing 0.1% Tween-20 and 4% fatty acid-free bovine serum albumin
596 in PBS buffer. Purified proteins (0.5 μg/mL, final concentration) were incubated with the PIP-strip
597 membranes for 1 h at room temperature and then washed three times using wash buffer containing
598 0.1% Tween-20 in PBS buffer. Bound proteins were detected by immunodetection of StrepII.
599 Lipids in the strip include phosphatidylinositol (4)-phosphate (PI(4)P), phosphatidylinositol (4,5)-
600 bisphosphate (PI(4,5)P2), phosphatidylinositol (3,4,5)-trisphosphate (PI(3,4,5)P3), triglyceride
601 (TRIG), diacylglycerol (DAG), phosphatidic acid (PA), phosphatidylserine (PS),
602 phosphatidylethanolamine (PE), phosphatidylcholine (PC), phosphatidylglycerol (PG), cardiolipin
603 (CL), phosphatidylinositol (PI), cholesterol (Cho), sphingomyelin (SM) and 3-
604 sulfogalactosylceramide (Sulfatide).

605

606 **Acknowledgments**

607 We thank the confocal microscopy facility at CAS Ecology/Center for Excellence in Molecular
608 Plant Sciences for technical supports. We thank Professor Jane Parker for providing *Nb epss* seeds.
609 L.W. was supported by National Key Laboratory of Plant Molecular Genetics, Institute of Plant
610 Physiology and Ecology/Center for Excellence in Molecular Plant Sciences and Chinese Academy
611 of Sciences Strategic Priority Research Program (Type-B; Project number: XDB27040214). X.L.
612 was supported by a Postdoc Grant (Project number: 2021M693172) from National Natural Science
613 Foundation of China. F.E-K. is supported by the German Research foundation (DFG Grants
614 CRC1101 D09 and EL 734/3-1). J.L.D. is supported by National Science Foundation (Grant IOS-
615 1758400) and HHMI. J.L.D. is a Howard Hughes Medical Institute (HHMI) Investigator. This
616 article is subject to HHMI's Open Access to Publications policy. HHMI lab heads have previously
617 granted a nonexclusive CC BY 4.0 license to the public and a sublicensable license to HHMI in
618 their research articles. Pursuant to those licenses, the author-accepted manuscript of this article can
619 be made freely available under a CC BY4.0 license immediately upon publication.

620 **References**

621

622 1. T. A. DeFalco, C. Zipfel, Review Molecular mechanisms of early plant pattern-triggered
623 immune signaling. *Mol Cell* **81**, 3449-3467 (2021).
624 2. J. D. Jones, R. E. Vance, J. L. Dangl, Intracellular innate immune surveillance devices in
625 plants and animals. *Science* **354** (2016).
626 3. P. Jacob *et al.*, Plant "helper" immune receptors are Ca2+-permeable nonselective
627 cation channels. *Science* **373**, 420-425 (2021).
628 4. L. M. Jubic, S. Saile, O. J. Furzer, F. El Kasmi, J. L. Dangl, Help wanted: helper NLRs and
629 plant immune responses. *Curr Opin Plant Biol* **50**, 82-94 (2019).
630 5. X. X. Liu, L. Wan, Molecular insights into the biochemical functions and signalling
631 mechanisms of plant NLRs. *Molecular Plant Pathology* **23**, 772-780 (2022).
632 6. D. Lapin *et al.*, A Coevolved EDS1-SAG101-NRG1 Module Mediates Cell Death Signaling
633 by TIR-Domain Immune Receptors. *Plant Cell* **31**, 2430-2455 (2019).
634 7. J. Gantner, J. Ordon, C. Kretschmer, R. Guerois, J. Stuttmann, An EDS1-SAG101 Complex
635 Is Essential for TNL-Mediated Immunity in Nicotiana benthamiana. *Plant Cell* **31**, 2456-
636 2474 (2019).
637 8. S. C. Saile *et al.*, Two unequally redundant "helper" immune receptor families mediate
638 Arabidopsis thaliana intracellular "sensor" immune receptor functions. *Plos Biology* **18**
639 (2020).
640 9. H. Adachi, L. Derevnina, S. Kamoun, NLR singletons, pairs, and networks: evolution,
641 assembly, and regulation of the intracellular immunoreceptor circuitry of plants. *Current*
642 *Opinion in Plant Biology* **50**, 121-131 (2019).
643 10. C. H. Wu *et al.*, NLR network mediates immunity to diverse plant pathogens. *Proc Natl*
644 *Acad Sci U S A* **114**, 8113-8118 (2017).
645 11. J. Wang *et al.*, Ligand-triggered allosteric ADP release primes a plant NLR complex.
646 *Science* **364** (2019).
647 12. G. Z. Bi *et al.*, The ZAR1 resistosome is a calcium-permeable channel triggering plant
648 immune signaling. *Cell* **184**, 3528-+ (2021).
649 13. J. Wang *et al.*, Reconstitution and structure of a plant NLR resistosome conferring
650 immunity. *Science* **364**, 1-11 (2019).
651 14. A. Forderer *et al.*, A wheat resistosome defines common principles of immune receptor
652 channels. *Nature* **610**, 532-539 (2022).
653 15. Y. B. Zhao *et al.*, Pathogen effector AvrSr35 triggers Sr35 resistosome assembly via a
654 direct recognition mechanism. *Sci Adv* **8**, eabq5108 (2022).
655 16. S. Horsefield *et al.*, NAD(+) cleavage activity by animal and plant TIR domains in cell
656 death pathways. *Science* **365**, 793-799 (2019).
657 17. S. Ma *et al.*, Direct pathogen-induced assembly of an NLR immune receptor complex to
658 form a holoenzyme. *Science* **370**, 1-10 (2020).
659 18. R. Martin *et al.*, Structure of the activated ROQ1 resistosome directly recognizing the
660 pathogen effector XopQ. *Science* **370**, 1-7 (2020).
661 19. S. Huang *et al.*, Identification and receptor mechanism of TIR-catalyzed small molecules
662 in plant immunity. *Science* **377**, eabq3297 (2022).

663 20. A. Jia *et al.*, TIR-catalyzed ADP-ribosylation reactions produce signaling molecules for
664 plant immunity. *Science* **377**, eabq8180 (2022).
665 21. L. Wan *et al.*, TIR domains of plant immune receptors are NAD(+)-cleaving enzymes that
666 promote cell death. *Science* **365**, 799-803 (2019).
667 22. K. Essuman, J. Milbrandt, J. L. Dangl, M. T. Nishimura, Shared TIR enzymatic functions
668 regulate cell death and immunity across the tree of life. *Science* **377**, 486-+ (2022).
669 23. X. H. Sun *et al.*, Pathogen effector recognition-dependent association of NRG1 with
670 EDS1 and SAG101 in TNL receptor immunity. *Nature Communications* **12** (2021).
671 24. Z. S. Wu, L. Tian, X. R. Liu, Y. L. Zhang, X. Li, TIR signal promotes interactions between
672 lipase-like proteins and ADR1-L1 receptor and ADR1-L1 oligomerization. *Plant*
673 *Physiology* **187**, 681-686 (2021).
674 25. Z. Gao, E. H. Chung, T. K. Eitas, J. L. Dangl, Plant intracellular innate immune receptor
675 Resistance to Pseudomonas syringae pv. maculicola 1 (RPM1) is activated at, and
676 functions on, the plasma membrane. *Proc Natl Acad Sci U S A* **108**, 7619-7624 (2011).
677 26. D. Qi, B. J. DeYoung, R. W. Innes, Structure-Function Analysis of the Coiled-Coil and
678 Leucine-Rich Repeat Domains of the RPS5 Disease Resistance Protein. *Plant Physiology*
679 **158**, 1819-1832 (2012).
680 27. Y. Belkhadir, Z. Nimchuk, D. A. Hubert, D. Mackey, J. L. Dangl, Arabidopsis RIN4
681 negatively regulates disease resistance mediated by RPS2 and RPM1 downstream or
682 independent of the NDR1 signal modulator and is not required for the virulence
683 functions of bacterial type III effectors AvrRpt2 or AvrRpm1. *Plant Cell* **16**, 2822-2835
684 (2004).
685 28. M. Hu, J. Qi, G. Bi, J. M. Zhou, Bacterial Effectors Induce Oligomerization of Immune
686 Receptor ZAR1 In Vivo. *Mol Plant* **13**, 793-801 (2020).
687 29. S. C. Saile *et al.*, Arabidopsis ADR1 helper NLR immune receptors localize and function at
688 the plasma membrane in a phospholipid dependent manner. *New Phytologist* **232**,
689 2440-2456 (2021).
690 30. C. Duggan *et al.*, Dynamic localization of a helper NLR at the plant-pathogen interface
691 underpins pathogen recognition. *Proc Natl Acad Sci U S A* **118** (2021).
692 31. Z. S. Wu *et al.*, Differential regulation of TNL-mediated immune signaling by redundant
693 helper CNLs. *New Phytologist* **222**, 938-953 (2019).
694 32. H. Adachi *et al.*, An atypical NLR protein modulates the NRC immune receptor network
695 in Nicotiana benthamiana. *PLoS Genet* **19**, e1010500 (2023).
696 33. H. Adachi *et al.*, An N-terminal motif in NLR immune receptors is functionally conserved
697 across distantly related plant species. *Elife* **8** (2019).
698 34. A. Schultink, T. Qi, A. Lee, A. D. Steinbrenner, B. Staskawicz, Roq1 mediates recognition
699 of the Xanthomonas and Pseudomonas effector proteins XopQ and HopQ1. *Plant J* **92**,
700 787-795 (2017).
701 35. S. Zhu *et al.*, SAG101 forms a ternary complex with EDS1 and PAD4 and is required for
702 resistance signaling against turnip crinkle virus. *PLoS Pathog* **7**, e1002318 (2011).
703 36. B. J. Feys *et al.*, Arabidopsis SENESCENCE-ASSOCIATED GENE101 stabilizes and signals
704 within an ENHANCED DISEASE SUSCEPTIBILITY1 complex in plant innate immunity. *Plant*
705 *Cell* **17**, 2601-2613 (2005).

706 37. J. Zonnchen *et al.*, EDS1 complexes are not required for PRR responses and execute TNL-
707 ETI from the nucleus in Nicotiana benthamiana. *New Phytol* **236**, 2249-2264 (2022).
708 38. M. Bernoux *et al.*, Subcellular localization requirements and specificities for plant
709 immune receptor Toll-interleukin-1 receptor signaling. *Plant Journal* 10.1111/tpj.16195
710 (2023).
711 39. M. Bernoux *et al.*, Comparative Analysis of the Flax Immune Receptors L6 and L7
712 Suggests an Equilibrium-Based Switch Activation Model. *Plant Cell* **28**, 146-159 (2016).
713 40. V. Markovic, Y. Jaillais, Phosphatidylinositol 4-phosphate: a key determinant of plasma
714 membrane identity and function in plants. *New Phytologist* **235**, 867-874 (2022).
715 41. Y. Dondelinger *et al.*, MLKL compromises plasma membrane integrity by binding to
716 phosphatidylinositol phosphates. *Cell Rep* **7**, 971-981 (2014).
717 42. Q. Chai *et al.*, A bacterial phospholipid phosphatase inhibits host pyroptosis by hijacking
718 ubiquitin. *Science* **378**, eabq0132 (2022).
719 43. Y. Zhong, Z. M. Cheng, A unique RPW8-encoding class of genes that originated in early
720 land plants and evolved through domain fission, fusion, and duplication. *Sci Rep-Uk* **6**
721 (2016).
722 44. D. C. Boyes, J. Nam, J. L. Dangl, The Arabidopsis thaliana RPM1 disease resistance gene
723 product is a peripheral plasma membrane protein that is degraded coincident with the
724 hypersensitive response. *P Natl Acad Sci USA* **95**, 15849-15854 (1998).
725 45. F. El Kasmi *et al.*, Signaling from the plasma-membrane localized plant immune receptor
726 RPM1 requires self-association of the full-length protein. *P Natl Acad Sci USA* **114**,
727 E7385-E7394 (2017).
728 46. B. P. M. Ngou, H. K. Ahn, P. T. Ding, J. D. G. Jones, Mutual potentiation of plant immunity
729 by cell-surface and intracellular receptors. *Nature* 10.1038/s41586-021-03315-7 (2021).
730 47. M. H. Yuan *et al.*, Pattern-recognition receptors are required for NLR-mediated plant
731 immunity. *Nature* 10.1038/s41586-021-03316-6 (2021).
732 48. R. N. Pruitt *et al.*, The EDS1-PAD4-ADR1 node mediates Arabidopsis pattern-triggered
733 immunity. *Nature* **598**, 495-+ (2021).
734 49. Y. J. Li *et al.*, Plasma membrane-nucleo-cytoplasmic coordination of a receptor-like
735 cytoplasmic kinase promotes EDS1-dependent plant immunity. *Nature Plants* **8**, 802-+
736 (2022).
737 50. H. N. Tian *et al.*, Activation of TIR signalling boosts pattern-triggered immunity. *Nature*
738 **598**, 500-+ (2021).
739 51. J. Kourelis *et al.*, The helper NLR immune protein NRC3 mediates the hypersensitive cell
740 death caused by the cell-surface receptor Cf-4. *PLoS Genet* **18**, e1010414 (2022).
741 52. H. K. Ahn *et al.*, Effector-dependent activation and oligomerization of plant NRC class
742 helper NLRs by sensor NLR immune receptors Rpi-amr3 and Rpi-amr1. *EMBO J*
743 10.15252/embj.2022111484, e111484 (2023).
744 53. M. P. Contreras *et al.*, Sensor NLR immune proteins activate oligomerization of their
745 NRC helpers in response to plant pathogens. *EMBO J* 10.15252/embj.2022111519,
746 e111519 (2022).
747 54. J. M. Feehan et al., Oligomerisation of a plant helper NLR requires cell-surface and
748 intracellular immune receptor activation. *P Natl Acad Sci USA* **120**, e2210406120 (2023).

749 55. X. Liu *et al.*, RIN13-mediated disease resistance depends on the SNC1-EDS1/PAD4
750 signaling pathway in Arabidopsis. *J Exp Bot* **71**, 7393-7404 (2020).
751 56. G. E. Crooks, G. Hon, J. M. Chandonia, S. E. Brenner, WebLogo: a sequence logo
752 generator. *Genome Res* **14**, 1188-1190 (2004).
753 57. F. W. Studier, Protein production by auto-induction in high density shaking cultures.
754 *Protein Expr Purif* **41**, 207-234 (2005).
755 58. Y. Durocher *et al.*, Scalable serum-free production of recombinant adeno-associated
756 virus type 2 by transfection of 293 suspension cells. *J Virol Methods* **144**, 32-40 (2007).
757

Supplementary figures

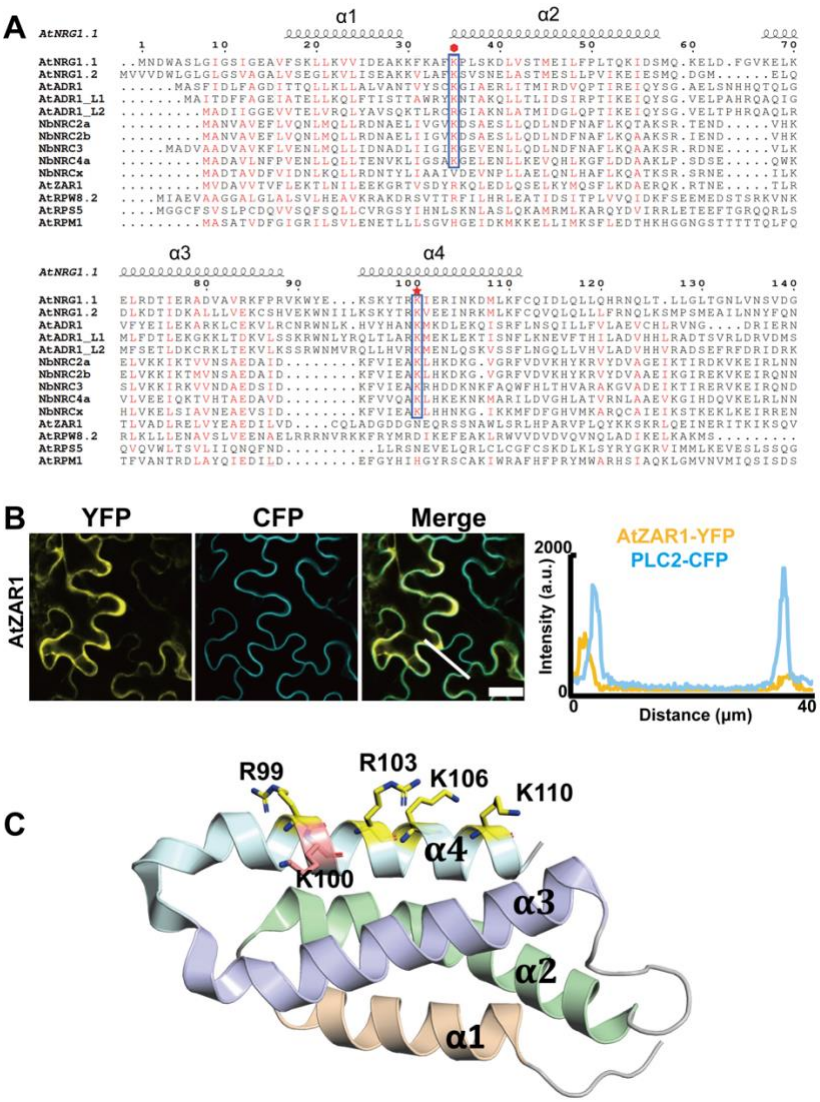

Figure S1 Identification of conserved positively charged residues in plant helper NLRs. **(A)** Sequence alignment in the CC^R and CC domains of helper NLRs and some sensor CNLs from Arabidopsis and *Nb*. The alignment was performed with ClustalX and the figure was prepared using ESPript. Red asterisk points to the position of AtNRG1.1 K100, and red hexagon points to the position of AtADR1_L1 K30. **(B)** Confocal assay showing that resting state AtZAR1 mainly localizes in the cytosol. Fluorescence intensities were measured along the white line depicted in the merge images. Bars, 25 μm. **(C)** Cartoon presentation of AtNRG1.1 CC^R structure (PDB:7L7W) with R99 K110, R103, K106 and K110 shown as sticks.

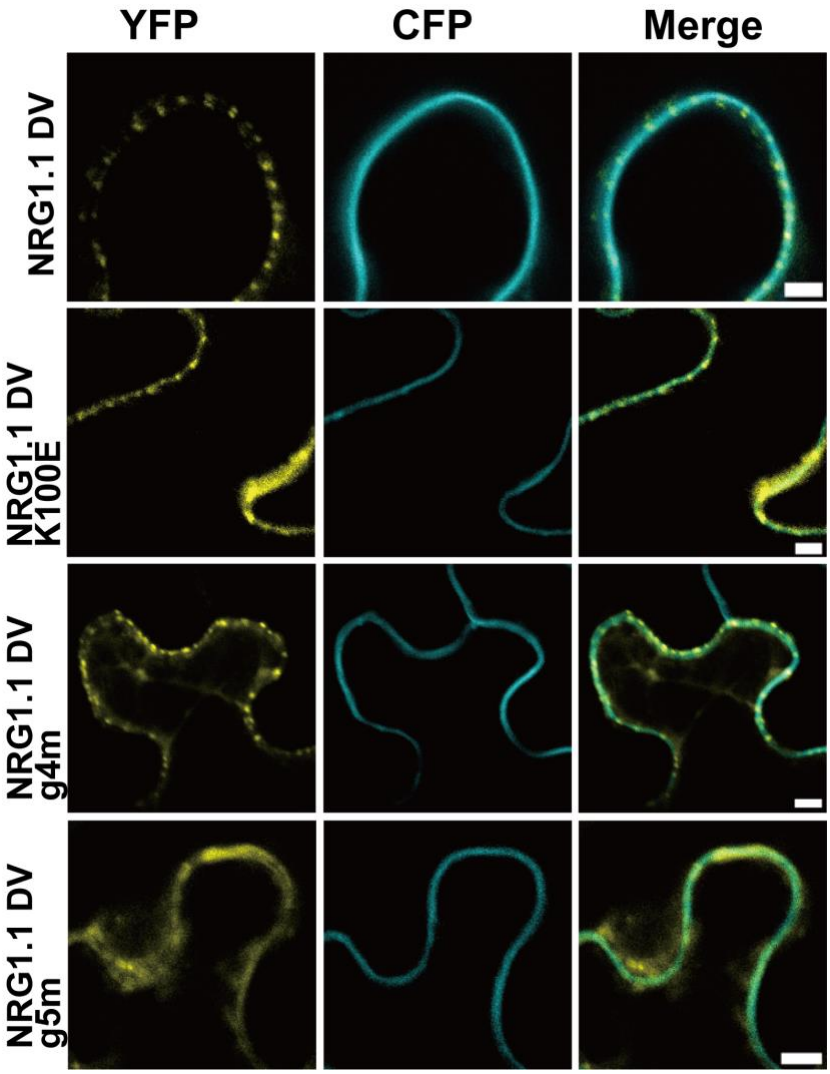

Figure S2 Peripheral images of the confocal assays in Figure 2C.

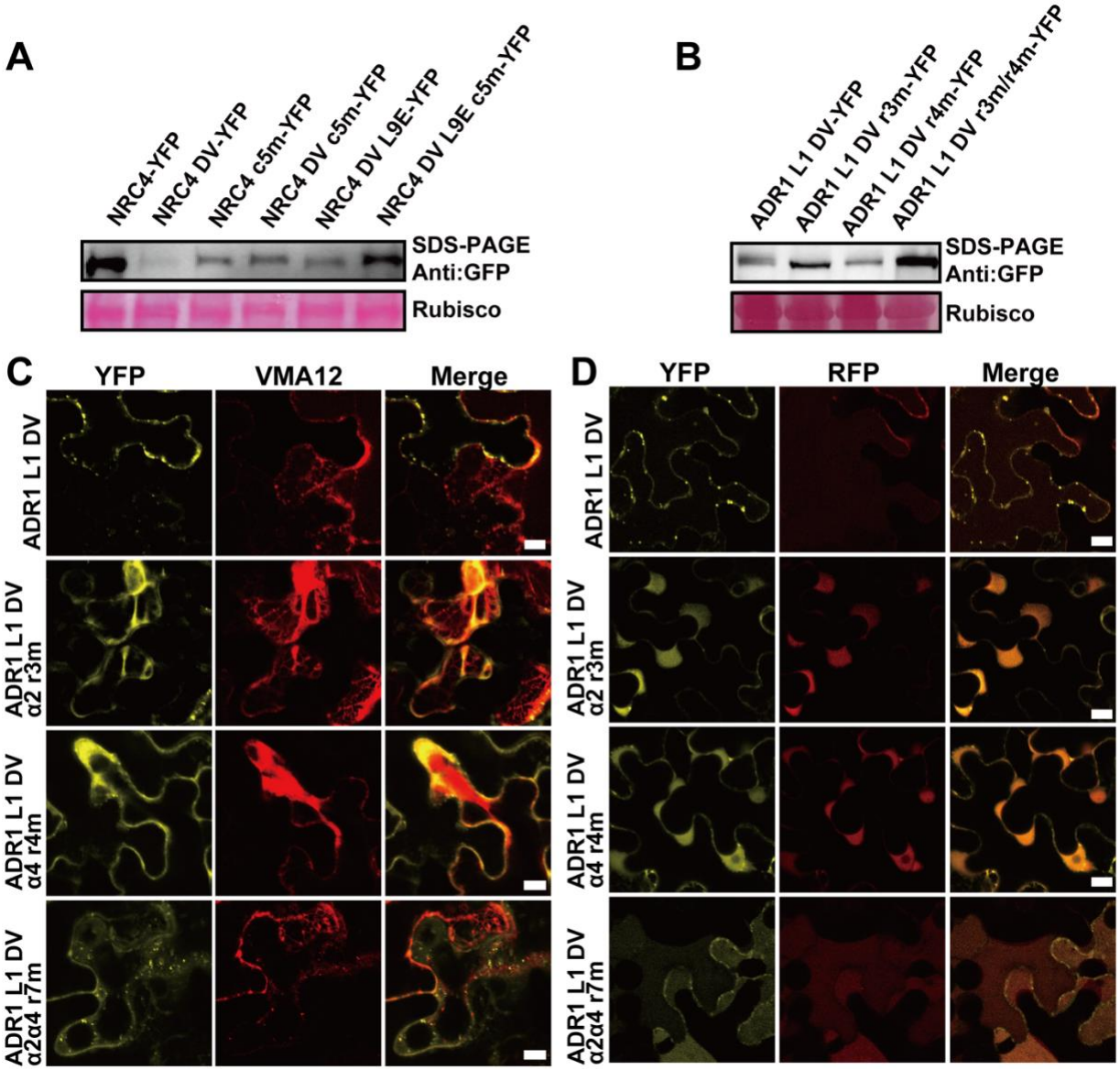

Figure S3 (A) Protein expression levels of NbNRC4 and NbNRC4 DV relevant mutants in Figure 3B. **(B)** Protein expression levels of AtADR1_L1 relevant mutants assayed by immunoblot. Confocal microscopy assays showing if the mis-localized ADR1_L1 DV mutants co-localize with the ER marker VMA12 (**C**) or cytosolic RFP (**D**). The indicated proteins fused with a C-terminal YFP were transiently co-expressed with the ER marker VMA12 fused to RFP or RFP in *Nb* leaves and confocal images were taken at 32-36h post infiltration. Confocal images are single plane secant views. Images are single plane secant views. Merge means merged images between YFP and RFP images.

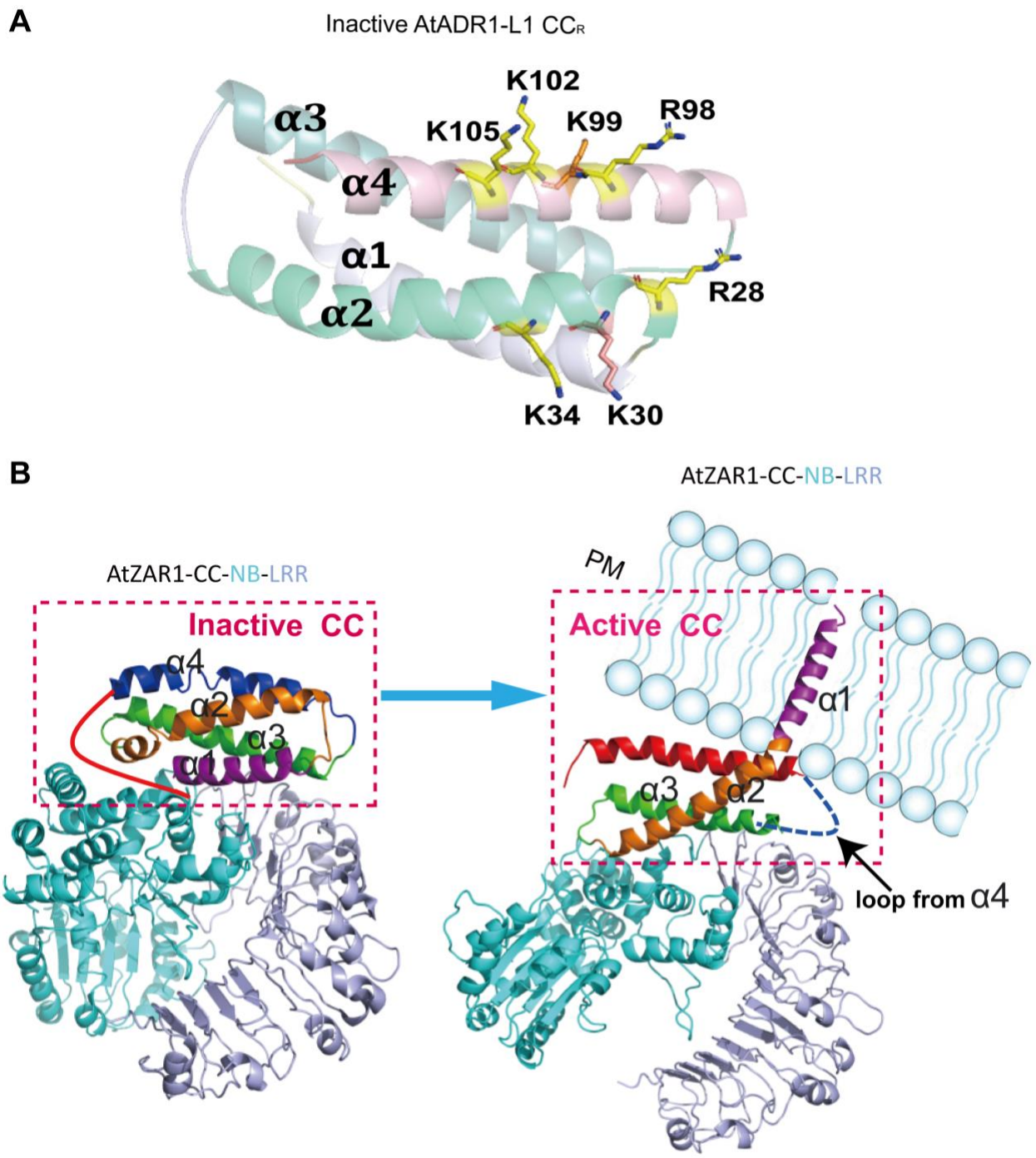

Figure S4 (A) Cartoon presentation of an AlphaFold AtADR1-L1 structure highlighting the positively charged residues involved in r3m and r4m. **(B)** Cartoon presentation of AtZAR1 in resting state (PDB: 6J5W) and in active state (PDB: 6J5T) highlighting the conformational changes in the CC domain and PM association.

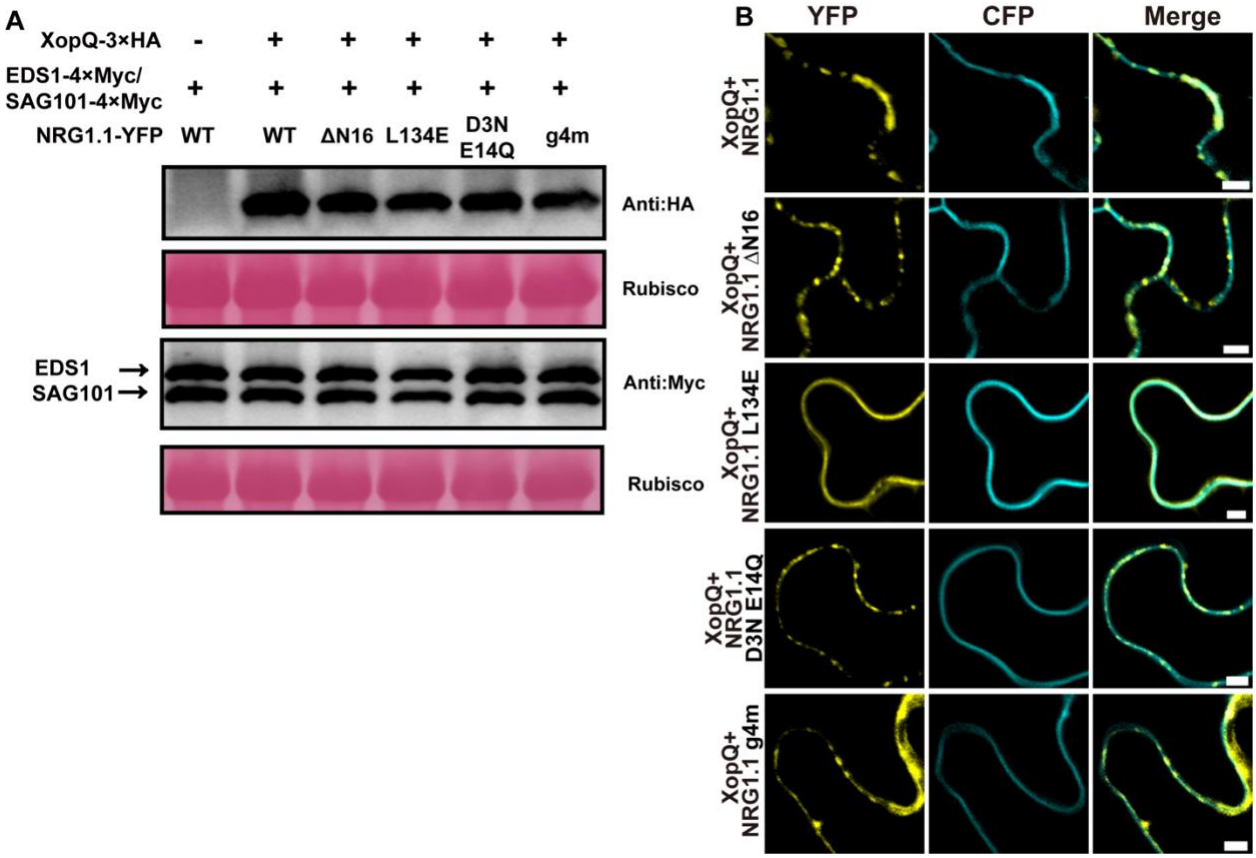

Figure S5 (A) Protein levels of XopQ, EDS1 and SAG101 from experiments displayed in Figure 5A and 4B. HA-tagged XopQ and Myc-tagged EDS1/SAG101 were separated by SDS-PAGE and blotted for anti-HA and anti-Myc, respectively. **(B)** Peripheral images of the confocal assays in Figure 5D-5H.

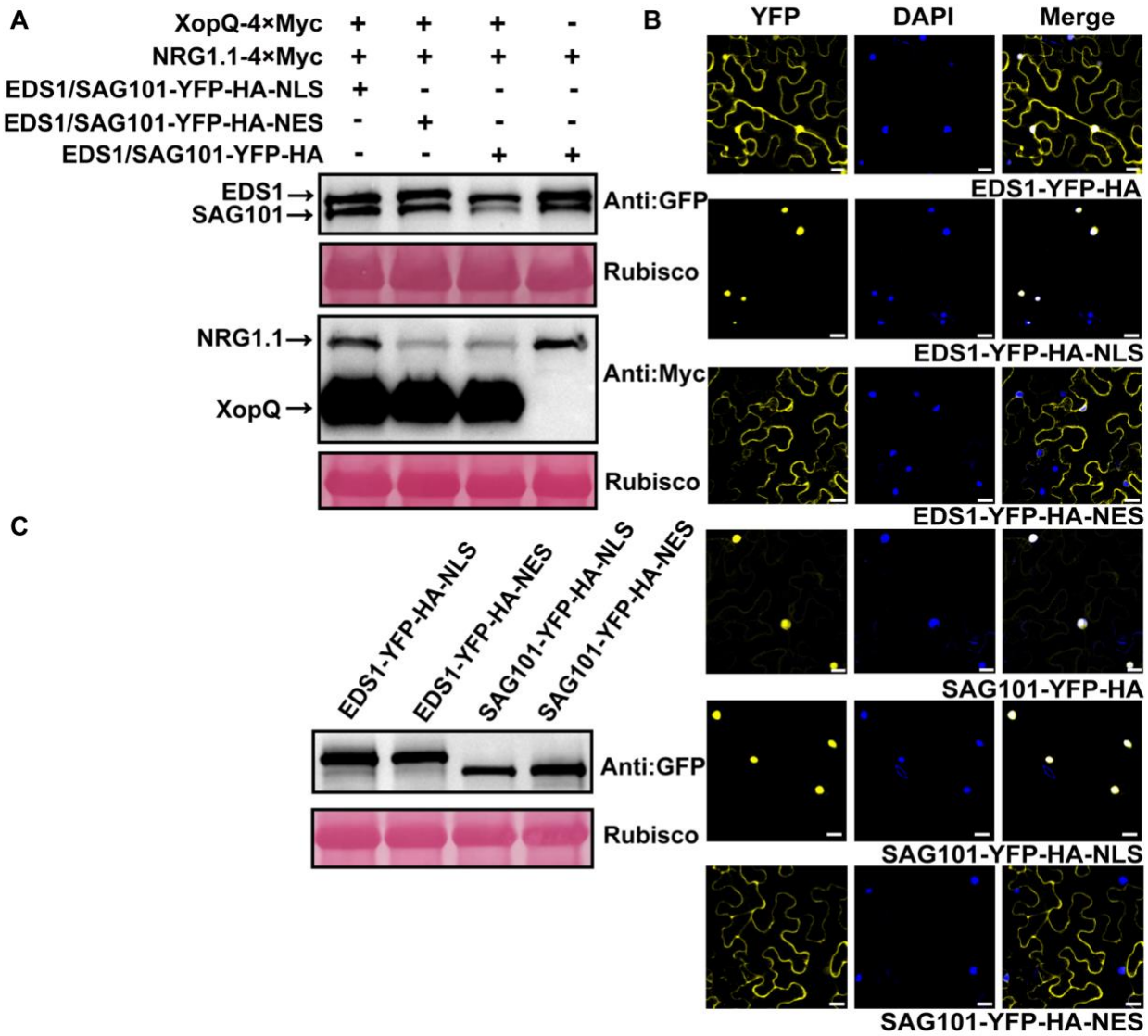

Figure S6 (A) Protein expression levels of samples from experiments displayed in Figure 6A. Total proteins were extracted from samples harvested at 26h post infiltration. Target proteins were separated by SDS-PAGE and blotted with the appropriate antibodies. **(B)** Confocal images showing the subcellular localization of EDS1-YFP-HA, EDS1-YFP-HA-NLS, EDS1-YFP-HA-NES, SAG101-YFP-HA, SAG101-YFP-HA-NLS and SAG101-YFP-HA-NES. Images were photographed at 48h post infiltration in *Nb* leaves. Nuclei were stained with DAPI (4', 6-diamidino-2-phenylindole). Bars, 20 μm. **(C)** Protein accumulation of samples in (B) detected with anti-GFP antibody.

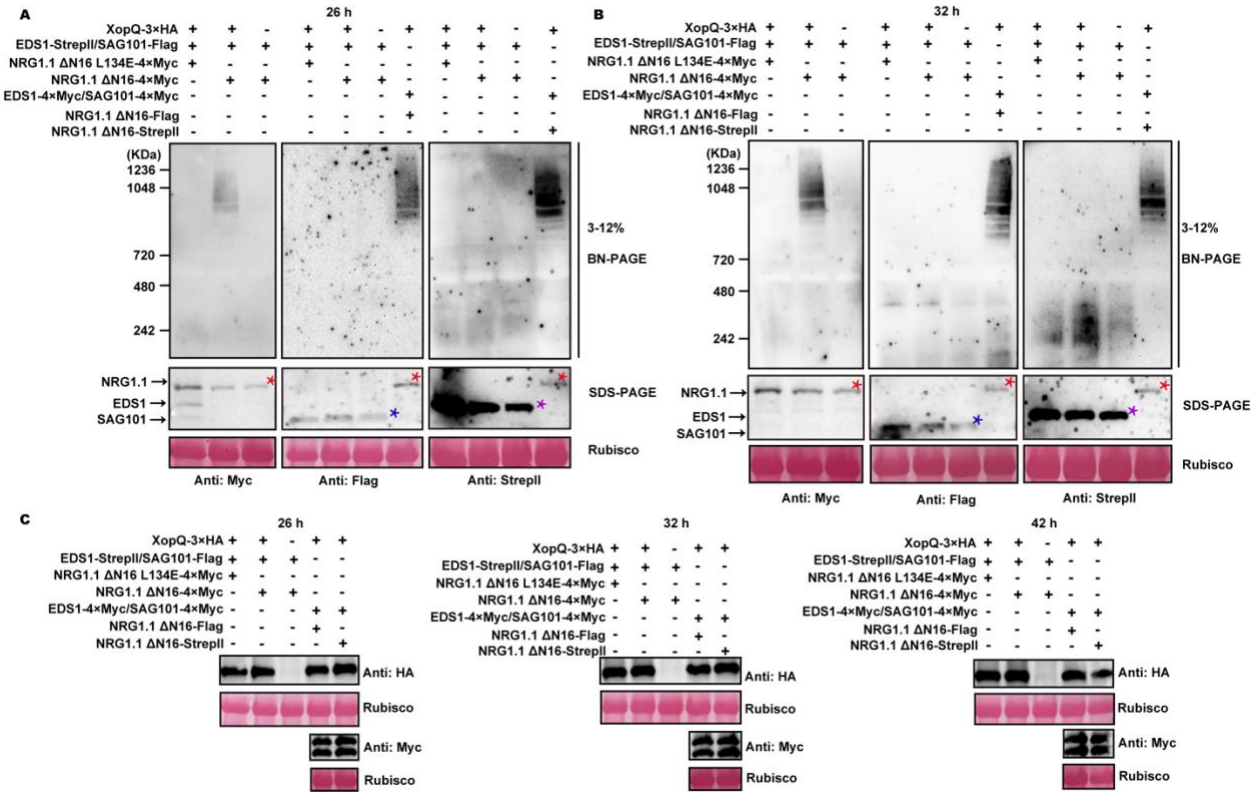

Figure S7 BN-PAGE assays showing that EDS1/SAG101 is not observed in an oligomeric complex with NRG1.1 at 26h **(A)** or 32h (**B)** after co-expression with XopQ in *Nb epss*. Red, purple and blue asterisks indicate NRG1.1, EDS1 and SAG101 bands, respectively. **(C)** Protein expression of XopQ, EDS1 and SAG101 as displayed in Figure 4B and Figure S5A and S5B was verified by SDS-PAGE. XopQ, EDS1/SAG101 were detected with anti-HA antibody and anti-Myc antibody, respectively.

Table S1 Gene ID of the 69 helper NLR homologs used in the alignment by CLustalW.

Gene	Gene ID (databases)[1]	Plant species
AtNRG1.1	At5g66900.1 (TAIR)	*Arabidopsis thaliana*
AtNRG1.2	At5g66910.1 (TAIR)	*Arabidopsis thaliana*
NbNRG1	NbS00018358g0013.1 (SGN)	*Nicotiana benthamiana*
AlNRG1	2614272850 (IMG)	*Arabidopsis lyrata*
AhNRG1	2614358615 (IMG)	*Arabidopsis halleri*
CrNRG1	2614531086 (IMG)	*Capsella rubella*
EhNRG1	2615507434 (IMG)	*Eutrema halophilum*
CsNRG1	2615787498 (IMG)	*Citrus sinensis*
CcNRG1	2614549921 (IMG)	*Citrus clementina*
PpNRG1	2615813723 (IMG)	*Prunus persica*
VvNRG1.1	649552880 (IMG)	*Vitis vinifera*
VvNRG1.2	649554972 (IMG)	*Vitis vinifera*
SpNRG1.1	2615336907(IMG)	*Salix purpurea*
SpNRG1.2	2615348770 (IMG)	*Salix purpurea*
RcNRG1	649572805 (IMG)	*Ricinus communis*
PtNRG1	2615290452 (IMG)	*Populus trichocarpa*
SlNRG1	Solyc02g090380.4.1 (SGN)	*Nicotiana benthamiana*
AtADR1	At1g33560.1 (TAIR)	*Arabidopsis thaliana*
AtADRL1 L1	At4g33300.1 (TAIR)	*Arabidopsis thaliana*
AtADRL1 L2	At5g04720.1 (TAIR)	*Arabidopsis thaliana*
NbADR1	Niben101Scf02422g02015.1 (SGN)	*Nicotiana benthamiana*
AlADR1	2614261905 (IMG)	*Arabidopsis lyrata*
AlADR1 L1	2614291476 (IMG)	*Arabidopsis lyrata*
AlADR1 L2	2614268259 (IMG)	*Arabidopsis lyrata*
AhADR1	2614369556 (IMG)	*Arabidopsis halleri*
CrADR1	2614512948 (IMG)	*Capsella rubella*
CrADR1 L1	2614509067 (IMG)	*Capsella rubella*
CrADR1 L2	2614505477 (IMG)	*Capsella rubella*
EhADR1	2615515499 (IMG)	*Eutrema halophilum*
EhADR1 L1	2615525947 (IMG)	*Eutrema halophilum*
EhADR1 L2	2615515499 (IMG)	*Eutrema halophilum*
GrADR1	2614796124 (IMG)	*Gossypium raimondii*
PtADR1	2615278681 (IMG)	*Populus trichocarpa*
CcADR1	2614532153 (IMG)	*Citrus clementina*
CsADR1	2615787425 (IMG)	*Citrus sinensis*
VvADR1	649539454 (IMG)	*Vitis vinifera*
SpADR1	2615316196 (IMG)	*Salix purpurea*
PpADR1	2615813687 (IMG)	*Prunus persica*
RcADR1	649560471 (IMG)	*Ricinus communis*
NbNRC2a	NbS00018282g0019.1 (SGN)	*Nicotiana benthamiana*
NbNRC2b	NbS00026706g0016.1 (SGN)	*Nicotiana benthamiana*
NbNRC3	NbS00011087g0003.1 (SGN)	*Nicotiana benthamiana*
NbNRC4a	NbS00002971g0007.1 (SGN)	*Nicotiana benthamiana*
NbNRC4b	NbS00016103g0004.1 (SGN)	*Nicotiana benthamiana*
NbNRCX	NbS00030243g0001.1 (SGN)	*Nicotiana benthamiana*
SlNRC1	Solyc01g090430.3.1 (SGN)	*Solanum lycopersicum*
SlNRC2	Solyc10g047320.2.1 (SGN)	*Solanum lycopersicum*
SlNRC3	Solyc05g009630.3.1 (SGN)	*Solanum lycopersicum*

Gene	Gene ID (databases)[1]	Plant species
SlNRC4a	Solyc04g007070.3.1 (SGN)	*Solanum lycopersicum*
SlNRC4b	Solyc04g007060.3.1 (SGN)	*Solanum lycopersicum*
SlNRC4c	Solyc04g007030.3.1 (SGN)	*Solanum lycopersicum*
SlNRCX	Solyc03g005660.4.1 (SGN)	*Solanum lycopersicum*
StNRC1a	PGSC0003DMT400066999 (SGN)	*Solanum tuberosum*
StNRC1b	PGSC0003DMT400066996 (SGN)	*Solanum tuberosum*
StNRC1c	PGSC0003DMT400066993 (SGN)	*Solanum tuberosum*
StNRC2a	PGSC0003DMT400080649 (SGN)	*Solanum tuberosum*
StNRC2b	PGSC0003DMT400080647 (SGN)	*Solanum tuberosum*
StNRC4a_1	PGSC0003DMT400041024 (SGN)	*Solanum tuberosum*
StNRC4a_2	PGSC0003DMT400069010 (SGN)	*Solanum tuberosum*
StNRC4a_3	PGSC0003DMT400069014 (SGN)	*Solanum tuberosum*
StNRC4a_4	PGSC0003DMT400041023 (SGN)	*Solanum tuberosum*
StNRC4b_1	PGSC0003DMT400019304 (SGN)	*Solanum tuberosum*
StNRC4b_2	PGSC0003DMT400019303 (SGN)	*Solanum tuberosum*
StNRC4b_3	PGSC0003DMT400019302 (SGN)	*Solanum tuberosum*
StNRC4b_4	PGSC0003DMT400019327 (SGN)	*Solanum tuberosum*
SmNRC1	SMEL4.1_12g003240.1 (SGN)	*Solanum melongena*
SmNRC3	SMEL4.1_10g001370.1 (SGN)	*Solanum melongena*
SmNRC4a	SMEL4.1_11g018090.1 (SGN)	*Solanum melongena*
SmNRC4b	SMEL4.1_11g018170.1 (SGN)	*Solanum melongena*

[1]TAIR, IMG and SGN are abbreviated from Arabidopsis Information Resource, Integrated Microbial Genomes and Solanaceae Genomics Network databases.